



Evaluation of DMSO as Working Fluid in Condensation Particle Counters

Sarah Kirchhoff^{1,2}, Patrick Weber¹, Oliver F. Bischof^{1,4}, Gerhard Steiner³, Christian Kunath³, Lothar Keck³, Victoria M. Fruhmann⁵, Helmut Krasa⁵, Alexander Bergmann⁵, Andreas Petzold^{1,2}, and Ulrich Bundke¹

¹Institute of Climate and Energy Systems 3 – Troposphere, Forschungszentrum Jülich GmbH, Jülich, Germany

²Institute for Atmospheric and Environmental Research, University of Wuppertal, Wuppertal, Germany

³GRIMM Aerosol Technik Ainring GmbH, Ainring, Germany

⁴TSI GmbH, Particle Instruments, Aachen, Germany

⁵Institute of Electrical Measurement and Sensor Systems, Graz University of Technology, Graz, Austria

Correspondence: Sarah Kirchhoff (sa.kirchhoff@fz-juelich.de) and Patrick Weber (p.weber@fz-juelich.de)

Abstract. This study presents a comprehensive laboratory and field-based evaluation of dimethyl sulfoxide (DMSO) as a non-flammable working fluid for condensation particle counters (CPCs), directly compared to a butanol-operated counterpart across a wide range of pressures, temperatures, and aerosol types. Modifications to the instrument's automatic refilling system ensured reliable operation over six months. Particle growth in the DMSO-CPC is strongly depending on the saturator temperature T_{sat} and the temperature difference ΔT between saturator and condenser, with optimal growth achieved at high T_{sat} and large ΔT values. Measurements with an optical particle counter downstream of the condenser, along with saturation and droplet size simulations, confirmed these trends and emphasized the importance of CPC internal settings for reliable particle growth. The DMSO-CPC achieved counting efficiencies and cutoff diameters comparable to the Butanol-CPC. The mean cutoff diameter was (5.8 ± 0.9) nm for the DMSO-CPC and (5.6 ± 0.5) nm for the Butanol-CPC. At the same time, the DMSO-CPC substantially reduced working fluid consumption and enabled stable long-term operation. The use of DMSO–H₂O mixtures further extended the operational range and improved safety, making the CPC suitable for airborne measurements and remote monitoring. Recommendations regarding instrument modification, operational conditions, and hardware adjustments are made for operating a DMSO-CPC to gain results comparable to a Butanol-CPC. Overall, DMSO-based CPCs provide safe, efficient, and regulation-compliant operation without compromising measurement quality under challenging environmental conditions.

1 Introduction

Aerosol particles play a crucial role in the Earth's atmosphere by influencing climate, weather patterns, air quality and human health (Pöschl, 2005; McNeill, 2017; IPCC, 2021). Their ability to scatter and absorb solar radiation, and to act as cloud condensation and ice nuclei, makes aerosols a key component of the global climate system (IPCC, 2021). Despite their importance, the sources, transformation processes and atmospheric distribution of aerosols remain highly uncertain, contributing significantly to the overall uncertainty in climate projections (Lee et al., 2016; Watson-Parris and Smith, 2022). High quality in-situ measurements of aerosol properties - in particular particle number concentrations - are essential to constrain models, validate



satellite retrievals and improve our understanding of aerosol-related processes at regional and global scales (Kahn et al., 2023). As aerosols span several orders of magnitude in size and vary in composition, a variety of measurement techniques has been developed. Each technique is based on different physical principles and optimized for particular particle size ranges and applications (Kulkarni et al., 2011; Wendisch and Brenguier, 2013).

Among the instruments available for aerosol number concentration measurements, Condensation Particle Counters (CPCs) are widely regarded as a gold standard (Balendra et al., 2024). CPCs can detect particles as small as a few nanometers in diameter. This makes them indispensable for a wide variety of research and monitoring applications. CPCs are routinely deployed in ground-based observatories to study new particle formation and urban pollution (Alam et al., 2003; Aalto et al., 2005). They are also operated on mobile platforms such as aircraft and drones to characterise vertical and horizontal aerosol distributions (Bundke et al., 2015; Petzold et al., 2015; Kim et al., 2025). And they are used in remote or high-altitude environments where particle concentrations are extremely low (Jurányi et al., 2010). CPCs are also integral to laboratory studies on instrument calibration, as well as to long-term climate monitoring networks and regulatory air quality assessments (Maring and Schwartz, 1994; Cozic et al., 2006). A leading example is the European research infrastructure ACTRIS (Aerosol, Clouds, and Trace Gases Research Infrastructure), encompassing over 100 research-performing organizations (Laj et al., 2024). Furthermore, the new EU Directive 2024/2881 of the European Parliament and the Council on ambient air quality and cleaner air for Europe (OJ EU, 2024/2881) establishes more stringent limit values for major air pollutants and requires the installation of at least one ultra fine particle concentration monitoring station per five million inhabitants.

However, deploying CPCs especially on aircraft has been challenging. Strict safety regulations limit the use of flammable working fluids, such as n-butanol or isopropanol, commonly used in these instruments (Weber et al., 2023). These fluids pose a fire hazard under the conditions typical of aircraft operation. This risk is especially pronounced in pressurized cabins or during high-altitude flights, leading to restrictions or outright prohibitions on their use in airborne applications (Hermann et al., 2005). Using water as a working fluid avoids the health and safety concerns associated with alcohol. However, water has two disadvantages that render it unsuitable for aircraft operation. First, it has a higher mass diffusion coefficient than butanol (Mei et al., 2021), which increases working fluid consumption during operation. Second, there is a risk of organic contamination during prolonged periods of inactivity.

In this study, we investigate a novel, non-flammable working fluid suitable for use in CPCs. Dimethyl-Sulfoxide (DMSO; C_2H_6OS ; CAS no. 67-68-5; 99.9%) as alternative fluid has been selected for its favorable thermodynamic properties, non-toxicity, odorless and compliance with aviation safety standards. A recent study (Weber et al., 2023) revealed that DMSO is a suitable working fluid with several advantages over butanol. They could show that the saturation vapor pressure of DMSO is significantly lower than that of butanol and water, while exhibiting an analogous temperature dependence. Consequently, the same supersaturation can be achieved with an identical temperature difference between the CPC's saturator and condenser. At the same time, the consumption of the working fluid is greatly reduced.



The D_{50} cutoff diameter, which represents the particle size at which a CPC detects 50% of incoming particles and thus defines its lower detection limit, is a key performance parameter of CPCs. Ambiguous results regarding the pressure dependence of the D_{50} cutoff diameter have been reported in studies using conventional working fluids. For butanol, Hermann and Wiedensohler (2001) found that there is a shift of the D_{50} towards smaller particle diameters and a decrease in the asymptotic maximum counting efficiency as the pressure decreases. In contrast, both theoretical and experimental studies (Zhang and Liu, 1990, 1991; Bauer et al., 2023) reported that lower pressures cause the D_{50} cutoff to shift toward larger particle sizes in butanol- and water-based CPCs. Bezantakos and Biskos (2022) found no significant influence of the pressure on the cutoff diameter with isopropyl alcohol as working fluid. Table 1 provides a comprehensive overview of the D_{50} cutoff diameters established in the various studies. The studies by Bundke et al. (2015), Bischof (2022), and Weber et al. (2023) were conducted using a similar experimental setup. While Bundke et al. (2015) reported a decrease in the cutoff diameter towards lower pressures, Bischof (2022) and Weber et al. (2023) found no significant pressure dependence for the D_{50} . A possible explanation for these ambiguous results are the different temperature settings of the CPCs. Bundke et al. (2015) adjusted the temperature difference of condenser and saturator to achieve a lower cut-off of 13 nm, while Bischof (2022) operated the CPC with internal temperatures as stated by the manufacturer ($T_{\text{sat}} = 36^\circ\text{C}$ and $T_{\text{con}} = 10^\circ\text{C}$). Besides that, a consensus has been reached among preceding studies that a shift of the D_{50} towards smaller particle sizes occurs as the temperature difference between the saturator and condenser of the CPC increases (Bezantakos and Biskos, 2022; Hermann and Wiedensohler, 2001; Mei et al., 2021).

It was shown by Weber et al. (2023) that, when DMSO is used as the working fluid, D_{50} is independent of both pressure and relative humidity within the measurement uncertainty for a saturator temperature of $T_{\text{sat}} = 40^\circ\text{C}$ and a condenser temperature of $T_{\text{con}} = 5^\circ\text{C}$. However, their study was limited to assessing the feasibility of DMSO as a working fluid. Continuous fluid supply and the effects of saturator and condenser temperature settings were not investigated. In this study, we build upon their work by evaluating the performance of a CPC operated with DMSO through laboratory characterisation and field-relevant measurements. Our focus includes droplet growth in the condenser, counting and cutoff efficiencies, operational long-term stability, and performance under varying temperature and pressure conditions. To support the interpretation of the experimental results, we conducted numerical simulations using a computational fluid dynamics (CFD) program.

2 Methods

2.1 Experimental Setup

2.1.1 Low-Pressure Characterisation

A schematic of the experimental setup for the low-pressure characterisation is shown in Fig. 1. Briefly, a constant and steady test aerosol production is provided by a continuous output nebuliser (model 3076, TSI Incorporated, Shoreview, MN, USA) or an inverted flame soot generator (Argonaut Scientific Corp., Edmonton, AB, Canada). The salt aerosol stream from the nebu-



Table 1. A comparison of the pressure dependency of the D_{50} cutoff diameter reported by different studies using various types of CPCs, working fluids, particles and internal temperature settings.

CPC type	TSI 7610 ^{[1]*}	GRIMM 5410 CEN ^[2]	TSI 3772 CEN ^[2]	TSI 3760 ^{[3]*}	TSI 3007 ^{[4]*}	GRIMM 5411 ^[5]	GRIMM 5411 ^[6]	GRIMM 5411 ^[7]
Aerosol type	Silver	Silver	Silver	NaCl	-	AS	AS	NaCl
Working fluid	n-butanol	n-butanol	n-butanol	n-butanol	Isopropyl alcohol	n-butanol	n-butanol	DMSO
p (hPa)	D_{50} (nm)							
1000	14	6.6	6.7	13	8			
900						14.9		
750		7.2	6.9					
700	13				8		8.1	5.6
600						12.8		
500		8.8	7.5				8.0*	6.0
400	12							
375		10.7						
300	11.5						8.0*	
250		22.6	8.9					
200	11.5			20		13.1	7.2	6.3
170						11.4		
160	11.5							
150			21.5					

^[1]Hermann and Wiedensohler (2001), ^[2]Bauer et al. (2023), ^[3]Zhang and Liu (1991), ^[4]Bezantakos and Biskos (2022), ^[5]Bundke et al. (2015)

^[6]Bischof (2022), ^[7]Weber et al. (2023)

* This data has been obtained from a graphical representation of the efficiency curves.

liser is dried in a diffusion dryer tube filled with silica gel. The dried stream, or the soot aerosol directly, is then passed through an aerosol neutraliser containing a radioactive source of Am-241. In the next step, a monodisperse aerosol stream is generated using a Vienna-type Differential Mobility Analyser (DMA; model M-DMA 55-U, GRIMM Aerosol Technik, Muldestausee, Germany). The DMA was operated step-wise, and each voltage level corresponded to a different particle size. The sizes ranged from an upper limit of 140 nm down to 2.5 nm in diameter. The monodisperse aerosol then enters the low-pressure section through a critical orifice. For operation at pressures above 700 hPa, the orifice is removed to ensure proper flow conditions. A characterization of the orifice is described in Bundke et al. (2015). The aerosol flow is diluted in a mixing chamber which also acts as a buffer volume. The pressure in the low-pressure section is controlled by mass flow balance using mass flow

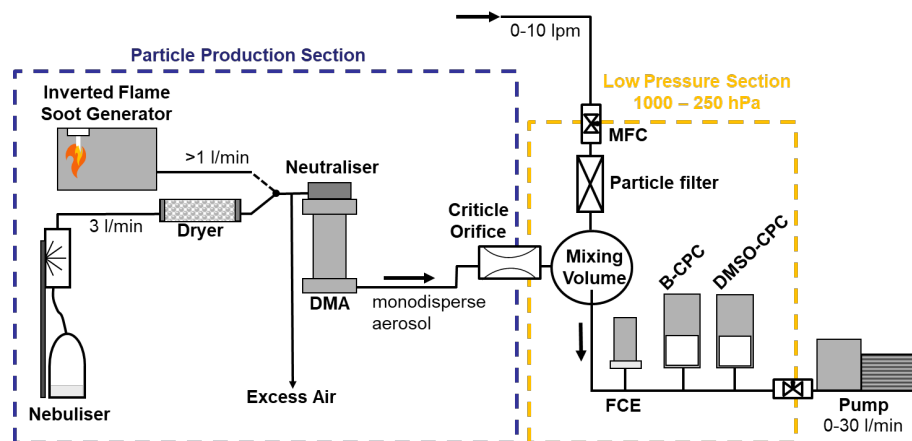


Figure 1. Schematic of the experimental setup for evaluating CPC performance under controlled low-pressure conditions. Test aerosols were generated either by a nebuliser producing salt particles (NaCl or $(\text{NH}_4)_2\text{SO}_4$) or by an inverted flame soot generator. The aerosol was dried, neutralised, and size-selected with a Differential Mobility Analyser (DMA) to produce a monodisperse stream. The flow then entered the low-pressure section through a critical orifice, where dilution and pressure control were achieved using a mixing chamber and mass flow controllers. Downstream, the aerosol was distributed to the reference Faraday Cup Electrometer (FCE), the butanol-based CPC (B-CPC), and the DMSO-CPC for parallel measurements. Original setup by Bundke et al. (2015), modified by and adapted from Weber et al. (2023).

100 controllers (MFCs) with a proportional-integral-derivative (PID) controller approach. After passing through the mixing chamber, the aerosol flow is delivered to the measuring instruments via a common sampling line. An individual isokinetic, isoaxial sample inlet in the centre of the line directs the aerosol flow to each instrument. To avoid particle losses due to electrostatic forces, all tubing and chambers are constructed of either stainless steel or minimum length conductive silicone tubing. The experiments are controlled automatically by a custom-made LabView™ (National Instruments Corp., Austin, TX, USA) program.

105 In order to investigate the performance of the CPC when utilising various aerosol types, the nebuliser was employed to nebulise salt solutions. Sodium chloride (NaCl) and ammonium sulfate (AS) were selected for this purpose. Furthermore, the measurement of fresh combustion soot was conducted. It should be noted that, unless stated otherwise, the test aerosol is NaCl .

110 Two Sky-CPC 5411 instruments (GRIMM Aerosol Technik) were used for all measurements. The Sky-CPC is a commercially available version of the standard GRIMM CPC, but is approved for use in aviation as it is made from specific aviation grade materials. One CPC was operated with butanol (B-CPC), as intended by the manufacturer; the other CPC was operated with DMSO as working fluid (DMSO-CPC). A Faraday Cup Electrometer (FCE; model 5705, GRIMM Aerosol Technik) was used as a reference instrument for particle concentration. A more detailed description of the experimental setup can be found in previous studies (Bundke et al., 2015; Bischof, 2022; Weber et al., 2023).



As a result of the findings from a recent study (Weber et al., 2023), some modifications had to be made to the DMSO-CPC. It was found that rubber parts of the refilling valve that are in direct contact with DMSO start swelling, which leads to a shutdown of the instrument's wetting system after some time. In particular, an o-ring and a stamp were causing those problems. To solve these issues, the rubber o-ring was replaced with a silicone o-ring and the stamp was intentionally soaked with DMSO to swell to its maximum and then cut back to its original size (see Weber et al. (2023) for details).

2.1.2 Final Particle Size Quantification

Because particle growth inside the condenser cannot be measured directly, experiments were carried out to quantify the final droplet size after the condenser. The laboratory setup is shown in Fig. B1 in the appendix. A specially designed and self-constructed saturator-condenser-unit was used for this purpose. The saturator comprised a metal tube (length = 10 cm, inner diameter = 2 cm) containing a manually DMSO-wetted wick. The chosen dimensions closely represent those of the CPC used in this study. A heating element was wrapped around the tube, allowing manual control of the saturator temperature.

For reasons of feasibility, the condenser dimensions used in this experiment were slightly smaller than those of the Sky-CPC. The condenser temperature was fixed at 5 °C for all measurements. The particle size was determined immediately downstream of the condenser using a Portable Optical Particle Counter (POPS). The original instrument design by Gao et al. (2016) was modified in our laboratory. Our custom-built POPS employs a 405 nm diode laser to count and size individual particles in the range 125 nm – 4 μm based on elastic light scattering.

All components of the setup were connected with conductive silicone tubing, with the tubing length minimized to reduce particle losses. The flow rate was maintained at 0.6 lpm, consistent with all other measurements in this study. All experiments were performed using laboratory air, as the objective was to obtain a general characterisation of the resulting droplet sizes and their behaviour under varying saturator temperatures.

2.2 Model Simulations

Direct observation of vapor saturation and droplet growth inside the CPC is not feasible. To support the interpretation of experimental measurements, we employed numerical simulations. These simulations were conducted using COMSOL Multiphysics®, a three-dimensional computational fluid dynamic simulation program (CFD).

A two-dimensional axisymmetric model of the saturator and condenser stages was developed, with geometries chosen to closely reflect the actual instrument. Within the saturator, a metal rod of radius 0.2 cm is located at the centerline. It is assumed that this metal rod also has the saturator temperature T_{sat} . An additional insulator stage was simulated between the saturator and condenser stage. The overall flow rate was set to 0.6 lpm, as specified for the CPC. Simulations were carried out under various pressure and internal temperature conditions. Temperature-dependent properties of the working fluids, including surface tension, density, vapor pressure, and gas-phase diffusion coefficient, were obtained from Yaw's Handbook for both DMSO and



butanol (Yaws, 2003). Atmospheric pressure effects were considered by modifying the diffusion coefficient of the working fluid in air and the carrier gas density, as lower pressure decreases gas density and proportionally increases the diffusion coefficient (Bauer et al., 2023).

150

The model couples laminar flow, heat transfer in fluids, and convective-diffusion modules to compute the temperature, velocity, and vapor concentration fields in the CPC. These fields are then passed to MATLAB for the calculation of the subsequent droplet growth inside the condenser (Hao et al., 2021). The minimum particle size that can be activated for condensation growth is given by the Kelvin equation, where σ is the surface tension, R the molar gas constant, T the temperature, S the supersaturation ratio, and ν_m the molar volume:

155

$$D_{p,\text{Kelvin}} = \frac{4\sigma\nu_m}{RT \ln S} \quad (1)$$

Due to the spatial variation of temperature, surface tension and saturation ratio, $d_{p,\text{Kelvin}}$ also varies at different locations of the condenser. When the required supersaturation ratio is reached for a specific radial position and particle size $d_{p,\text{Kelvin}}$ according to eq. 1, droplet growth computation is initialized and solved using MATLAB's *ode15s* solver. This solver is designed to handle stiff differential equations and differential-algebraic equations (DAEs) with a variable-order integration method. A more in-depth description of the particle growth rate can be found in Pandis and Pandis (2016). Concentration-dependent effects, such as vapor depletion and condensational heating, are not considered in the simulation, as they become significant only at high particle number concentrations (Lewis and Hering, 2013). Vapor depletion refers to the uptake of working fluid vapor by particles, while condensational heating arises from the release of latent heat during condensation, which increases the local temperature and reduces the supersaturation. A more detailed description of the model can be found in Krasa et al. (2025).

160

165

3 Data Analysis Procedure

The raw data obtained from the experimental setup for low-pressure characterisation (Sect. 2.1.1) requires a series of corrections and adjustments before meaningful analysis can be performed. Figure 2 summarises the data analysis procedure, outlining the steps taken to correct and adjust the measurements and ultimately determine the counting efficiency of both CPCs.

170

The data analysis procedure described in this section was performed using an in-house developed Python program. The fully automated program applies all necessary corrections and adjustments, generating output files with the relevant parameters and producing several plots for graphical visualisation of the results.

3.1 Faraday Cup Electrometer

Accurate interpretation of Faraday Cup Electrometer (FCE) measurements requires correction of the raw data for instrumental offsets and pressure-dependent flow variations. The electrical offset of the FCE arises from small background currents within the electrometer circuitry or leakage currents in the measurement system. Offsets of a few femtoamperes (fA) are commonly

175

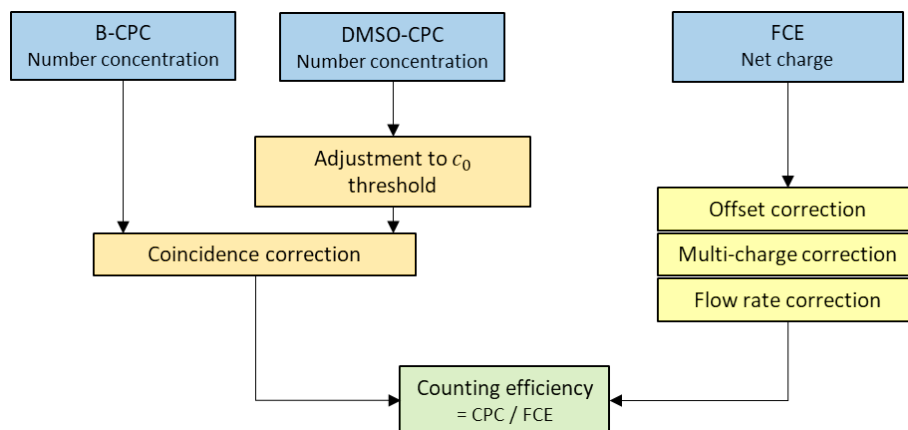


Figure 2. Overview of the data processing and correction workflow for the low-pressure characterisation experiments. The flowchart illustrates the sequential steps applied to the raw measurement data (blue), including correction, adjustment, and evaluation procedures (orange/yellow), leading to the determination of the counting efficiency for both CPCs (green). Adapted from Bischof (2022).

observed and can be comparable in magnitude to the aerosol-induced signal, especially under conditions of low particle concentration (Hermann et al., 2005; Jarrett and Owen, 2013). Consequently, regular baseline measurements with particle-free
 180 air must be performed to determine and subtract the offset current from the recorded data. Proper correction for this offset is essential to ensure the accuracy of the derived charge fluxes and to avoid systematic bias in the aerosol charge or concentration estimates. Furthermore, corrections to the electrometer flow rates were made to account for the corresponding conditions of reduced pressure.

185 When using a diffusion charger together with a DMA and an FCE as the reference instrument, it is important to account for the presence of multiple charged particles exiting the DMA. A particle carrying n charges will be detected n times by the FCE, whereas the CPC will register it only once. To correct for this discrepancy in counting rates, the procedure described by Bundke et al. (2015) was applied. This method incorporates the actual particle size distribution to properly account for the contribution of multiple charged particles.

190 The FCE instrument was not calibrated immediately prior to the measurements. According to the manufacturer, the calibration factor typically does not exceed 2%, indicating only a minor contribution to overall measurement uncertainty. Moreover, because we normalise our efficiency curves using the linearity of concentration signal (see Sect. 3.3), any systematic offset associated with the FCE calibration factor is effectively incorporated into this normalisation procedure. As a result, the absence
 195 of an externally applied FCE calibration factor is not expected to influence the interpretation of our results, especially the cutoff diameters.

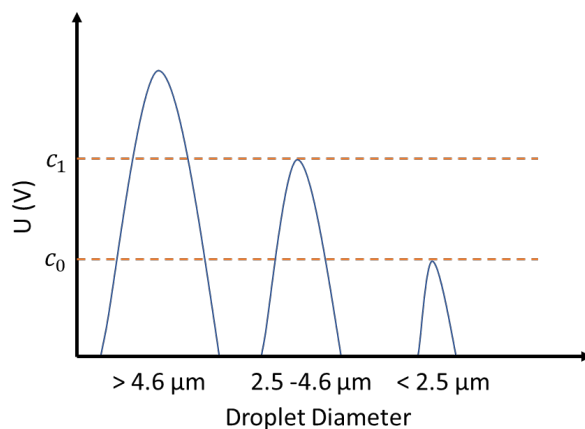


Figure 3. Illustration of the CPC detection thresholds $Th(c_0)$ and $Th(c_1)$ and their corresponding DMSO droplet diameters used to interpret the particle growth signal ratio c_1/c_0 (Fig. 6 of Weber et al. (2023)).

3.2 Particle Growth Adjustment

The Sky-CPC 5411 reports an internal diagnosis of the particle growth, displayed as the c_1/c_0 value. Here, $Th(c_1) = 1.2\text{ V}$ and $Th(c_0) = 0.5\text{ V}$ are internal voltage thresholds of the specific CPC model, and c_1 and c_0 are the corresponding numbers of particle counts. These thresholds are encoded in the hardware of the instrument and can not be changed by the user. Particles whose signal meets and exceeds the $Th(c_1)$ -threshold are counted and reported as number concentration c_1 by the CPC. Signals only surpassing the $Th(c_0)$ -threshold but not the $Th(c_1)$ -threshold are counted as c_0 . A ratio of $c_1/c_0 < 1$ therefore means that not all particles have grown sufficiently to reach $Th(c_1)$. As illustrated in Fig. 3, the diameters of DMSO droplets that correspond to the thresholds of c_0 and c_1 are $2.5\mu\text{m}$ and $4.6\mu\text{m}$ respectively. DMSO droplets smaller than $2.5\mu\text{m}$ are not counted. Weber et al. (2023) derived these values from the signal heights of latex test particles and a model that describes the scattered light intensity as a function of particle diameter for the GRIMM measuring cell. As these voltage thresholds were determined for butanol as working fluid by the manufacturer an adjustment for the use with DMSO has to be applied. This adjustment accounts for the low vapour pressure of DMSO, which results in less vapour being available for the condensation growth of the particles. It should be implemented in the instruments hardware by the manufacturer. As a workaround in this study, we use the c_0 -count as particle number concentration.

3.3 Linearity of Concentration Signal

The linearity of the concentration signal of a CPC describes how its measured response varies with changes in total particle number concentration relative to a reference instrument. Calibration is necessary due to the specific configuration and instrumentation used in this study. Figure 4 shows the linear relationships between the concentrations measured by both CPCs and the FCE, characterised by the slope K_0 . The black dashed line represents the 1 : 1 relationship, while the shaded gray area

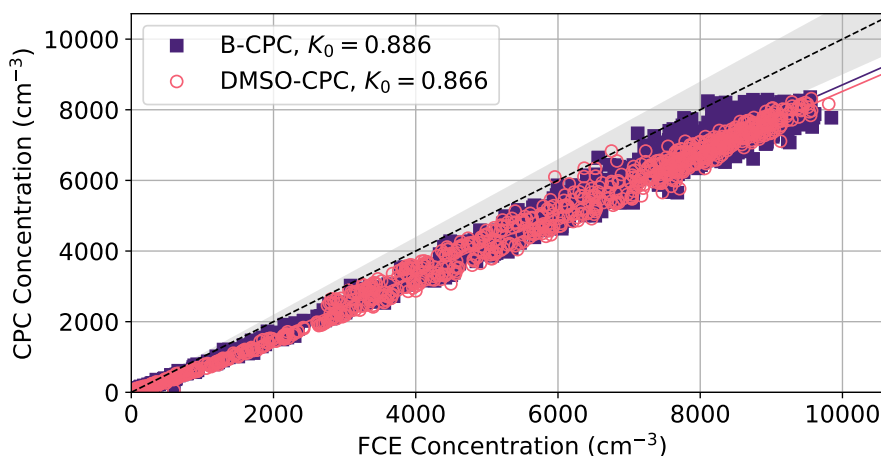


Figure 4. Comparison of the linearity of concentration signal of the B-CPC and DMSO-CPC with the electrometer reference for NaCl test aerosols. The black dotted line indicates the 1:1 relationship, and the grey band represents a $\pm 10\%$ deviation.

indicates a $\pm 10\%$ deviation. Filled squares correspond to the coincidence-corrected concentrations of the B-CPC, and circles denote the coincidence-corrected and c_0 -adjusted concentrations of the DMSO-CPC. Both datasets are plotted against the fully corrected FCE concentration. The slope obtained for the B-CPC is $K_0 = 0.886$, which agrees well with the slope of the DMSO-CPC, for which $K_0 = 0.866$. The slope of each linear fit is subsequently used to correct the data, ensuring comparability of the D_{50} cutoff diameters across all measurements by normalising the efficiency curves to unity (see Sect. 3.4).

3.4 CPC Counting Efficiency and Cutoff Diameter

In order to ascertain the performance of a CPC, the counting efficiency curve with respect to a reference instrument is utilised. The calculation of the particle-size-dependent counting efficiency η is derived from the ratio of the corrected number concentration of particles detected by the CPC (N_{CPC}) to the corrected number concentration measured by the reference instrument, in this case the electrometer (N_{FCE}):

$$\eta(D_p) = \frac{N_{\text{CPC}}}{N_{\text{FCE}}} \quad (2)$$

Figure 5 presents representative counting efficiency curves for the Sky-CPC 5411 operated with butanol and DMSO. The efficiency curves are parameterized by an exponential fit function introduced by Wiedensohler et al. (2018):

$$\eta_{\text{fit}}(D_p) = A \left(1 - \exp \left(\frac{B - D_p}{C - B} \ln 2 \right) \right) \quad (3)$$

From the efficiency curves, two characteristic parameters can be determined. First, the asymptotic maximum counting efficiency η_{max} . It represents the plateau region where the counting efficiency remains constant as the particle diameter increases. Second, the cutoff diameters, D_{50} and D_{90} , which correspond to the particle diameters at which 50% or 90% of the particles are counted relative to the reference.

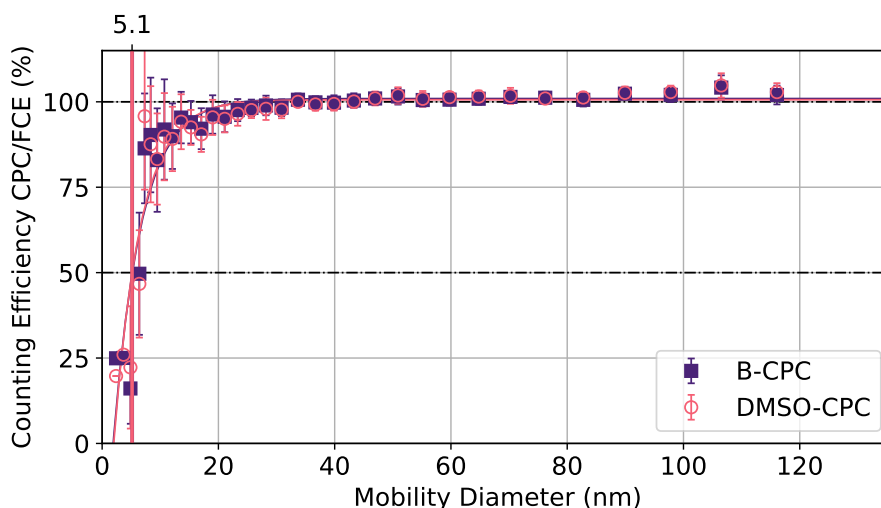


Figure 5. Counting efficiency curves for NaCl particles with respect to the electrometer reference instrument after all applied corrections for the B-CPC (squares) and the DMSO-CPC (circles) at 700 hPa, a saturator temperature of 40 °C, and a condenser temperature of 10 °C. Both CPCs exhibit a cutoff diameter of $D_{50} = 5.1$ nm.

4 Results & Discussion

235 4.1 Particle Growth

4.1.1 Evaluation of the CPC Internal Diagnosis (c_1/c_0)

The internal diagnosis of the GRIMM CPC associated with droplet growth is represented by the c_1/c_0 ratio, as illustrated in Sect. 3.2. The ratio is always found to fall between zero and one. It has been determined that a ratio of $c_1/c_0 < 1$ corresponds to DMSO droplets with diameters between 2.5 and 4.6 μm , whilst a ratio of $c_1/c_0 = 1$ indicates that the DMSO droplets have grown to diameters above 4.6 μm .

Table 2 summarizes the average c_1/c_0 ratios of the DMSO-CPC across all pressure and internal temperature settings. Each reported value represents the mean and standard deviation calculated from independent experiments. Although the c_1/c_0 values are not always constant during individual measurements and tend to exhibit systematic trends (see below), the overview of the average values serves to highlight the main features of droplet growth under varying conditions. The data show that droplet growth in the DMSO-CPC depends strongly on the internal temperature settings. The most efficient growth occurs at high saturator temperatures T_{sat} and large temperature differences ΔT . For $T_{\text{sat}} = 40$ °C and $\Delta T \geq 30$ °C, the c_1/c_0 ratio remains larger than 0.5. Reducing the temperature difference or the saturator temperature leads to consistently lower c_1/c_0 values across all pressures. However, the c_1/c_0 ratios at the reduced saturator temperature are exceptionally low for 1000 hPa and 250 hPa, with values as low as 0.03. Similarly low values occur at a saturator temperature of $T_{\text{sat}} = 40$ °C when the temperature difference is



Table 2. Average c_1/c_0 values for all pressure and temperature settings (in °C) of the DMSO-CPC.

p (hPa)	40/5	40/10	40/15	35/5	35/10
1000	0.93 ± 0.09	0.59 ± 0.34	0.14 ± 0.07	0.08 ± 0.04	0.08 ± 0.03
700	1.00 ± 0.01	0.98 ± 0.01	0.85 ± 0.01	0.65 ± 0.02	0.22 ± 0.01
500	1.00 ± 0.00	1.00 ± 0.01	0.93 ± 0.03	0.85 ± 0.02	0.33 ± 0.06
250	0.98 ± 0.01	0.89 ± 0.01	0.18 ± 0.01	0.08 ± 0.01	0.03 ± 0.01

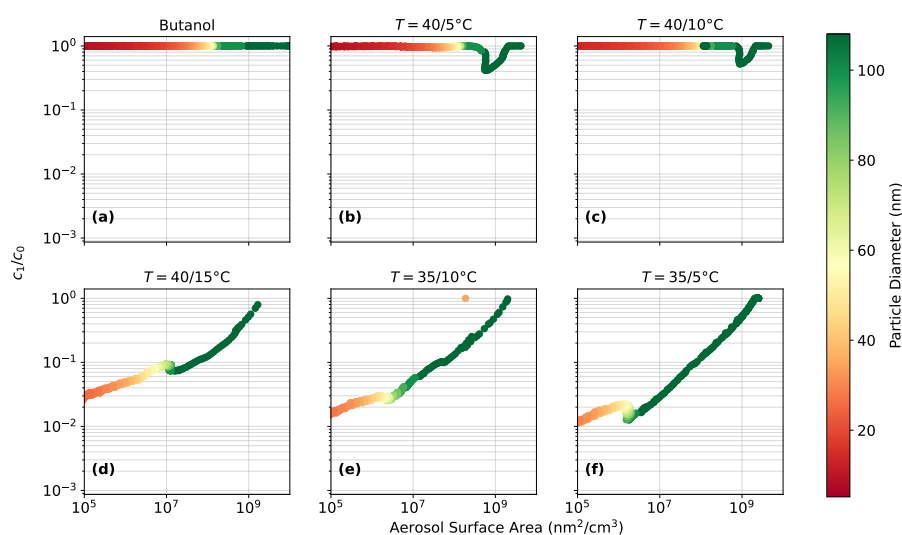


Figure 6. c_1/c_0 ratios versus total aerosol surface area at 1000 hPa. Colors indicate the initial particle diameter. (a) Butanol: $c_1/c_0 \approx 1$ across all surface areas. (b–f) DMSO: optimal temperature settings (b, c) maintain $c_1/c_0 \approx 1$, while non-optimal settings (d–f) show decreasing c_1/c_0 with smaller surface areas. The kink near $d_p \approx 50$ nm reflects the peak of the NaCl size distribution, indicating growth is limited by process duration rather than vapor availability.

reduced to $\Delta T = 25$ °C.

The graphical representation of the c_1/c_0 ratios as a function of the total aerosol surface area offers valuable insights into the condensational droplet growth mechanism. Figure 6 shows the c_1/c_0 values plotted against the total aerosol surface area at 1000 hPa and various temperature settings. Each panel represents one measurement cycle of the DMA. The color scale depicts the initial particle diameter of the monodisperse aerosol generated by the DMA. Panel (a) presents the results obtained with butanol as the working fluid averaged over all internal temperature settings. The c_1/c_0 ratio remains constant at unity, demonstrating that droplet growth is always sufficient to surpass both thresholds. The remaining panels present results obtained with DMSO as the working fluid under five combinations of saturator and condenser temperatures.



At optimal temperature settings, meaning high saturator temperatures and large temperature differences (panels (b) and (c)), the c_1/c_0 values remain close to unity for all surface areas. The little dip near an aerosol surface area of $10^9 \text{ nm}^2/\text{cm}^3$ is reproducible but no physical explanation has been identified. Across all non-optimal temperature settings (panels (d–f)), the overall trend of the c_1/c_0 ratio remains consistent. Non-optimal refers to conditions yielding c_1/c_0 values below 0.3 at any point during the measurement. The c_1/c_0 values reach unity for large aerosol surface areas but decline progressively with decreasing surface area. A slight kink is visible in the yellow region around $d_p \approx 50 \text{ nm}$, coinciding with the maximum of the size distribution of the generated NaCl test aerosol (see Weber et al. (2023)). That means at around $d_p \approx 50 \text{ nm}$ most particles are generated and towards both smaller and larger particle sizes the generated particle number concentration declines. This behaviour suggests that the droplet growth is not constrained by the availability of vapour, but rather by the duration of the process. Consequently, especially the smaller particles lack sufficient time to undergo substantial growth.

To validate this hypothesis, we conducted an experiment with a high aerosol number concentration at 250 hPa , $T_{\text{sat}} = 40^\circ\text{C}$ and $T_{\text{con}} = 10^\circ\text{C}$, as these conditions also produce the characteristic c_1/c_0 trend (see Fig. 7a). The results of the high-concentration experiment are shown in Fig. 7b. The high concentration represents a doubling of the aerosol number concentration compared to the original measurement. The kink at $d_p \approx 50 \text{ nm}$, now appears towards lower c_1/c_0 values with increasing surface area. This change in behaviour resulting from a higher aerosol number concentration indicates that a total aerosol surface area exceeding approximately $10^8 \text{ nm}^2/\text{cm}^3$ leads to a vapor-limited regime, where droplet growth is insufficient due to a limited availability of condensable vapor under these conditions. This validates our hypothesis that, during the regular measurements, the observed trend of the c_1/c_0 ratios can be explained by a time-limited regime in which the particles do not spend sufficient time in the condenser to grow to full droplet size.

The study conducted by Weber et al. (2023) did not report such low c_1/c_0 ratios under any conditions. The key difference between our study and the study conducted by Weber et al. (2023) lies in the DMSO supply. While Weber et al. (2023) manually wetted the wick inside the CPC with DMSO, we operated the CPC as intended by the manufacturer, with the CPC measuring the liquid level and automatically regulating the working fluid supply. With values as low as $\overline{c_1/c_0} = 0.03$, the required level of droplet growth is not achieved inside the DMSO-CPC, indicating that the automated DMSO supply of the CPC is not sufficient and leads to lower supersaturations and therefore to less or even insufficient particle activation under specific conditions. However, sufficient droplet growth is achieved with the current settings of the refilling process when T_{sat} and ΔT are high. In addition, the application of the c_0 -adjustment to ensure the comparability of all data (Sect. 3.2) could result in a considerable degree of uncertainty for low c_1/c_0 -ratios.

4.1.2 POPS Measurement of Final Droplet Size

To quantify the final droplet size at the outlet of the condenser, a series of measurements was performed using the experimental setup described in Sect. 2.1.2. The resulting DMSO droplet size distributions at three temperature differences are shown in Fig. 8. Panel (a) corresponds to the Sky-CPC temperature setting of $T_{\text{sat}} = 40^\circ\text{C}$ and $T_{\text{con}} = 5^\circ\text{C}$, which yielded the highest c_1/c_0

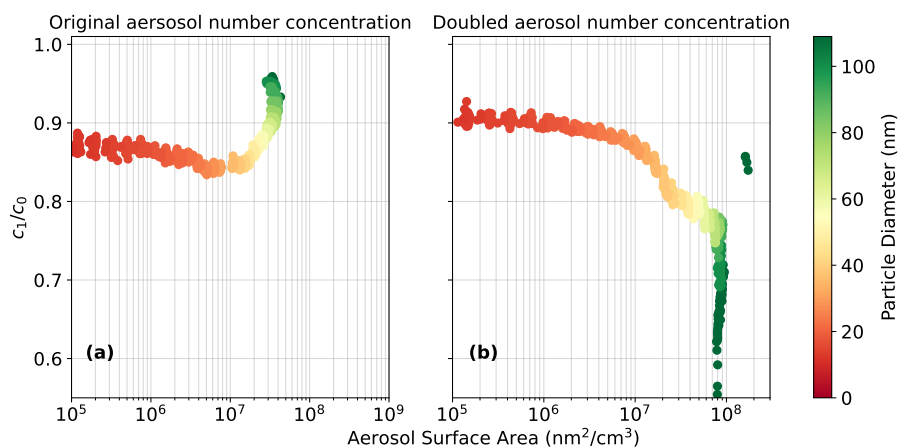


Figure 7. c_1/c_0 ratios versus total aerosol surface area at 250 hPa, $T_{\text{sat}} = 40^\circ\text{C}$, $T_{\text{con}} = 10^\circ\text{C}$ for a high-concentration aerosol experiment. Doubling the aerosol number concentration flips the kink near $d_p \approx 50$ nm to lower c_1/c_0 values at high surface areas, indicating a transition to a vapor-limited growth regime.

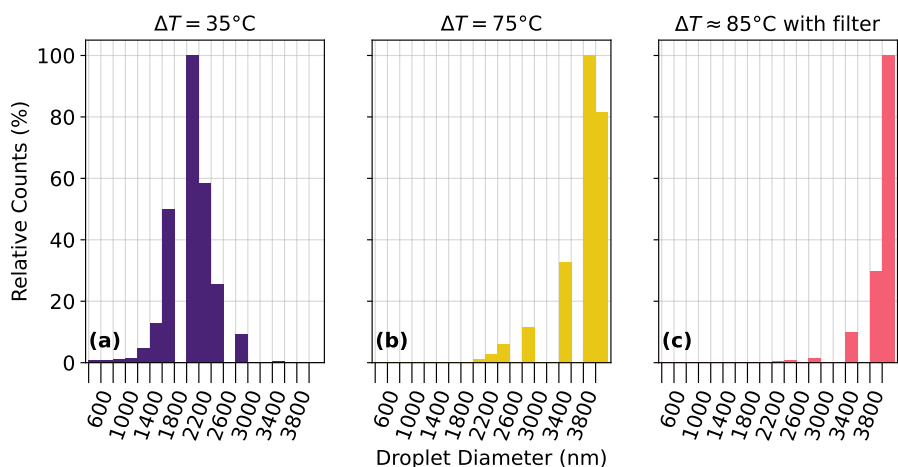


Figure 8. Final DMSO droplet size distributions at three temperature differences (ΔT). The condenser temperature was fixed at $T_{\text{con}} = 5^\circ\text{C}$. Relative particle counts as a function of droplet diameter were measured using a POPS. Panels (a) and (b) show results without a filter, while (c) shows measurements with a filter, indicating homogeneous nucleation.

295 ratios at ambient pressure (see Sect. 4.1.1). Those high ratios with $\overline{c_1/c_0} \approx 1$ indicate sufficient droplet growth to final droplet diameters larger than $4.6\ \mu\text{m}$ (see Fig. 3). However, the final droplet size distribution measured by POPS yields a count median diameter (CMD) in the size bin between 2000 nm and 2200 nm.

The significant difference between the c_1/c_0 -derived final droplet size and the POPS measurements can be attributed to two



300 factors. First, the geometric dimensions of the condenser in this setup differ from those of the Sky-CPC. Although the Sky-CPC
condenser is not directly accessible, we estimate it to be larger than the condenser used in the POPS measurements. Lewis and
Hering (2013) demonstrated that condenser diameter strongly affects the final droplet size, with wider tubes producing larger
droplets. Second, the difference in droplet size can also be explained by Mie theory, as the lower refractive index of DMSO
compared to polystyrene latex (PSL) particles affects light scattering and the inferred size. The POPS instrument operates at a
305 wavelength of $\lambda = 405$ nm. The refractive indices of DMSO and PSL at this wavelength are 1.49 and 1.59, respectively. Note
that the refractive index of DMSO at this wavelength was estimated via the dispersion relation for DMSO at 20 °C (Polyanskiy,
2024). Although this dispersion relation is an approximation and may vary with temperature, the lower refractive index of
DMSO relative to PSL implies that the measured size distribution would shift slightly toward larger particle diameters. This
shift was not quantified in our study. Instead, we focused on comparing the order of magnitude and general trends of the POPS
310 data under different CPC temperature settings.

Since the self-built CPC setup allows for higher saturator temperatures than the Sky-CPC, additional experiments were con-
ducted at larger temperature differences to determine the achievable operating range—that is, to assess how droplet growth is
affected and at which temperatures homogeneous nucleation of DMSO begins. Panel (b) shows the droplet size distribution
315 at $\Delta T = 75$ °C. The distribution shifts markedly towards larger droplet sizes, with a CMD in the size bin between 3600 nm
and 3800 nm. As expected, larger temperature differences between the saturator and condenser result in more pronounced
droplet growth. This shift would, in principle, also lead to smaller cutoff diameters. However, this could not be verified because
aerosols smaller than 5 nm could not be generated with our laboratory setup.

320 A further increase in the temperature difference to $\Delta T = 85$ °C results in homogeneous nucleation of DMSO. Panel (c) presents
the corresponding size distribution, obtained with a filter placed upstream of the saturator. Even under these particle-free con-
ditions, droplets larger than 4 μ m were detected, confirming homogeneous nucleation of DMSO under these conditions. It is
worth noting that, when the filter was installed, the droplet size counts for the measurements at $\Delta T = 35$ °C and $\Delta T = 75$ °C
dropped to zero.

325 4.2 Simulations

To validate the experimentally quantified final droplet size in the condenser (Sect. 4.1.1 & 4.1.2), model simulations of the sat-
uration ratio and droplet growth were conducted. The temperature and vapour pressure fields were simulated for the Sky-CPC
5411 operated with butanol and DMSO, as described in Sect. 2.2. From the results, the calculation of the saturation ratio S
was performed, which are presented as contour plots in Fig. 9 for the pressure stages of 1000 hPa, 500 hPa 250 hPa and for a
330 temperature setting of $T_{\text{sat}} = 40$ °C and $T_{\text{con}} = 10$ °C. The simulations were performed for all pressure stages and temperature
settings of the experimental results (see Sect. 4.3 and 4.4), but for clarity only those conditions are provided.

Figure 9 shows that both working fluids produce nearly identical saturation profiles when operated under identical condi-

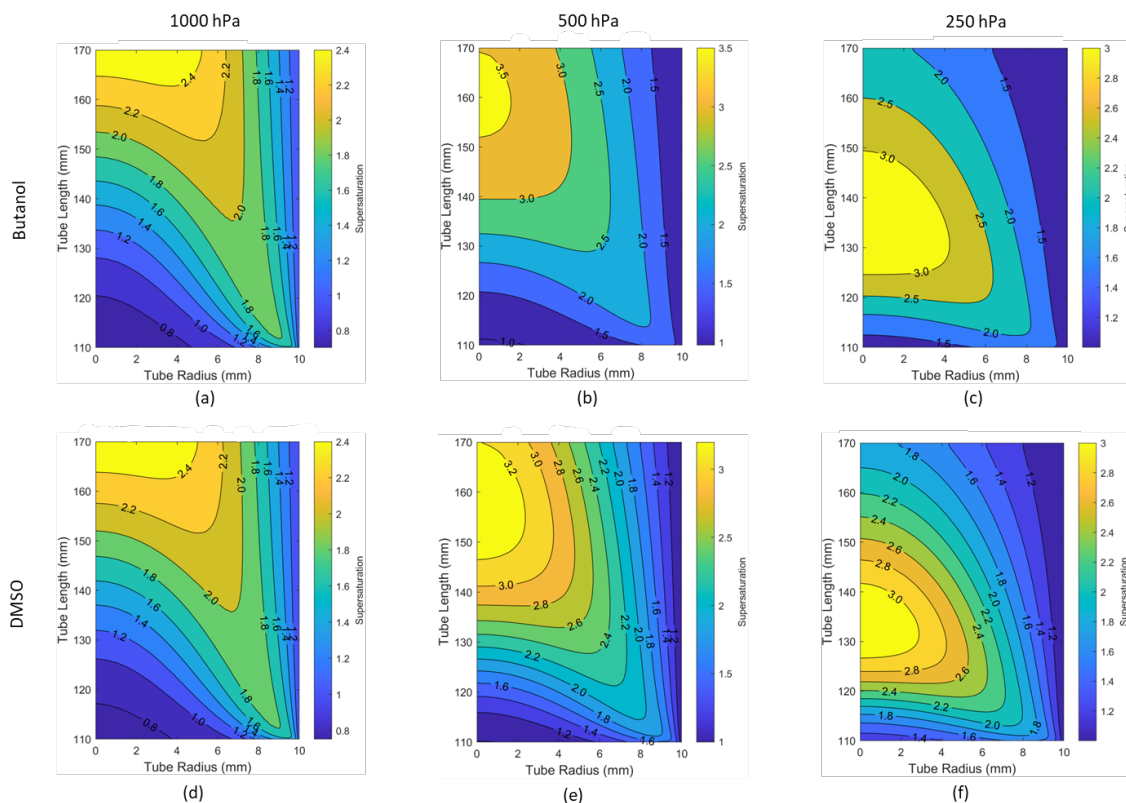


Figure 9. Simulated supersaturation of the CPC’s condenser for $T_{\text{sat}} = 40^\circ\text{C}$ and $T_{\text{con}} = 10^\circ\text{C}$ under various pressures. Panels (a - c) show the results for the B-CPC and panels (d - f) for the DMSO-CPC. The region of maximum saturation S_{max} , which controls the activation of the smallest particles, shifts toward the condenser center with decreasing pressure and reaches its highest value at 500 hPa. The profiles for both fluids are nearly identical under the same conditions.

tions. This consistency holds across all simulated temperature and pressure settings. A key feature of the profiles is the region of maximum saturation ratio S_{max} , which determines the smallest particles that can be activated. The position of S_{max} depends on pressure: at 1000 hPa, it occurs near the end of the condenser, while at lower pressures it shifts progressively toward the center. This trend agrees with previous simulation studies and can be attributed to the pressure dependence of the Reynolds number Re in the heat and mass transfer equations (Hermann et al., 2005; Bauer et al., 2023). Furthermore, the magnitude of S_{max} varies with pressure, being lowest at 1000 hPa and highest at 500 hPa. The low supersaturation observed at 1000 hPa may be attributed to the limited dimensions of the condenser. Owing to its short length, the system does not allow sufficient residence time for the maximum supersaturation to be reached. Furthermore, the longer mean free path at lower pressures enhances diffusion away from the liquid surface, leading to higher saturation ratios. At the lowest pressure stage (250 hPa), however, the supersaturation decreases again due to the reduced number of vapor molecules available.

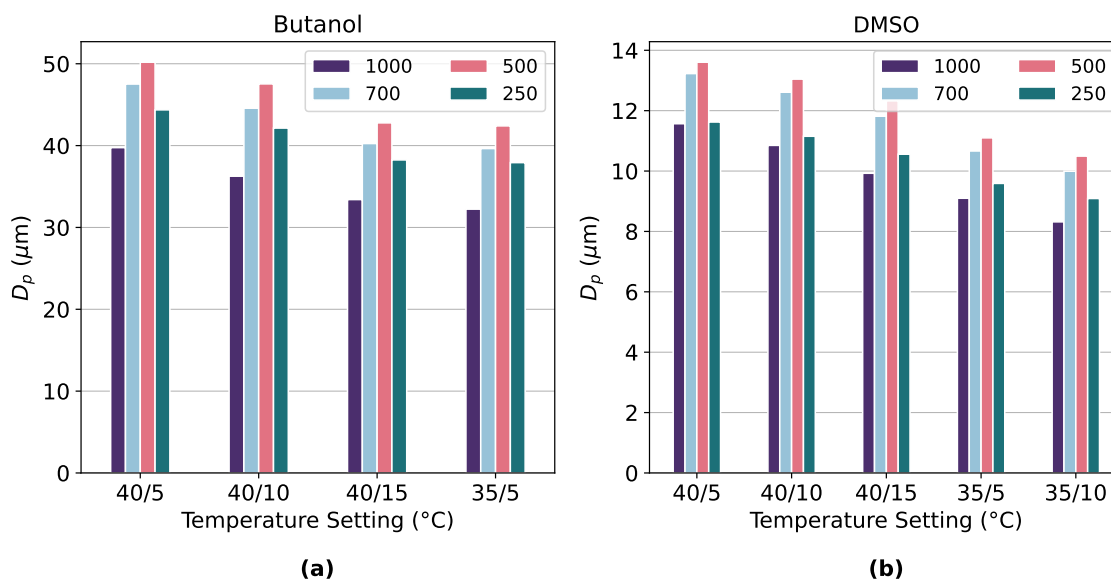


Figure 10. Simulated final droplet sizes for both working fluids across different temperatures and pressures. Droplet growth is larger in the B-CPC than the DMSO-CPC due to the higher saturation vapor pressure of butanol. Growth is smallest at 1000hPa, peaks at 500hPa, and decreases slightly at 250hPa. Larger temperature differences ΔT and higher saturator temperatures T_{sat} enhance droplet growth for both fluids.

345 The final droplet sizes resulting from the simulated saturation profiles were calculated for all temperature and pressure settings. The results are shown in Fig. 10 for both working fluids. Consistent with the lower saturation vapor pressure of DMSO compared to butanol, droplets in the B-CPC exhibit approximately four times greater growth than those in the DMSO-CPC, although the overall behaviour remains similar. The pressure-dependent droplet growth follows the same trend as the saturation profiles: the smallest growth occurs at 1000hPa, reaches a maximum at 500hPa, and decreases slightly at 250hPa. This pattern is observed for both working fluids across all temperature settings. Comparison of the different temperature conditions confirms two main trends derived from the experimental results. First, a larger temperature difference between the saturator and condenser ΔT leads to enhanced droplet growth. Second, for the same ΔT , a higher saturation temperature T_{sat} also promotes greater droplet growth. This is consistent with previous studies, where similar behaviour was observed (Krasa et al., 2025).

355 However, the simulated absolute final droplet sizes do not match the measured droplet sizes discussed in Sect. 4.1.1. While the c_1/c_0 values suggest insufficient droplet growth for DMSO under most conditions (see Table 2), the simulated final droplet diameters exceed $8\mu\text{m}$ for all conditions. Two potential explanations can be proposed for this discrepancy. First, the simulations assume a perfectly wetted wick and account solely for condensation processes. Because the freezing point of DMSO is 18°C , sublimation of the vapor may occur, which is not captured by the simulations. Second, we were limited to using estimated condenser dimensions as input for the numerical calculations in our study. Lewis and Hering (2013) demonstrated that the con-

360

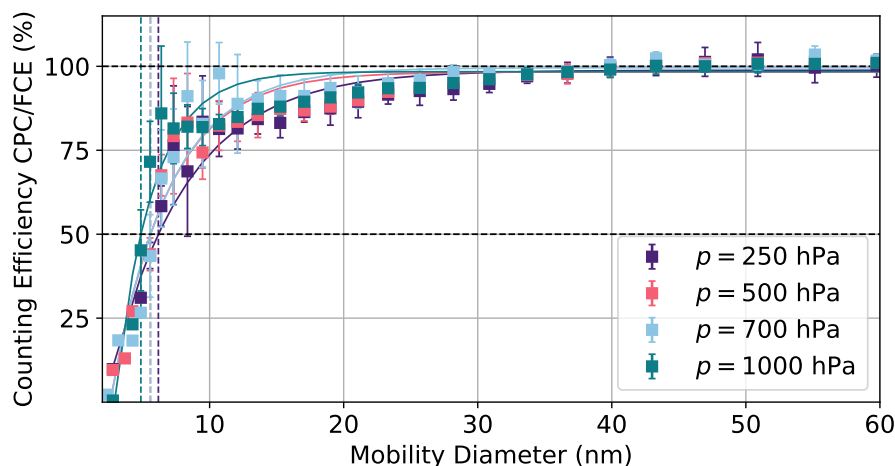


Figure 11. Counting efficiency curves of the DMSO-CPC at four pressures. Error bars denote the standard deviation of mean efficiencies. Dashed lines indicate calculated D_{50} cutoff diameters, which show no significant dependence on pressure.

denser diameter strongly affects droplet growth, with larger diameters yielding larger droplets. Also, their simulations similarly over-predicted droplet sizes compared to their experimental measurements. Accordingly, we may overestimated the Sky-CPC's geometric dimensions, leading to larger simulated droplet sizes. Nevertheless, the overall trends and the comparison between working fluids, temperature settings, and other studies support the validity of the results.

365 4.3 Pressure Dependency of the CPC Counting Efficiency

With the experimental setup described in Sect. 2.1.1 the counting efficiencies for two Sky-CPCs 5411 were determined at four different pressures of 1000, 700, 500 and 250 hPa. One CPC was operated with butanol as working fluid (B-CPC), the other with DMSO (DMSO-CPC). The chosen temperature setting for the DMSO-CPC corresponds to the setting where it was found to perform best, especially regarding its c_1/c_0 ratio which indicates sufficient particle growth. The saturator temperature of the DMSO-CPC was 40 °C, the temperature at the condenser 5 °C. The saturator temperature of the B-CPC was 36 °C, the temperature at the condenser 10 °C as intended by the manufacturer. The obtained counting efficiency curves are shown in Fig. 11. The y-axis error bars indicate the standard deviation of the counting efficiency mean values and the vertical dashed lines represent the calculated D_{50} cutoff diameters.

375 The asymptotic maximum counting efficiency η_{\max} is normalised to unity due to the applied calibration (see Sect. 3.3). Consequently, it is not possible to directly evaluate the dependence of η_{\max} on pressure. However, to assess this dependence, the slope correction parameters, K_0 , can be compared, while the D_{50} cutoff diameters remain directly comparable across different measurement conditions. Figure 11 shows a slight shift in the D_{50} towards larger particle diameters, which is associated with a less steep slope as the pressure decreases. This shift is negligible, as it moves the cutoff from $D_{50}(1000\text{hPa}) = 4.9\text{ nm}$

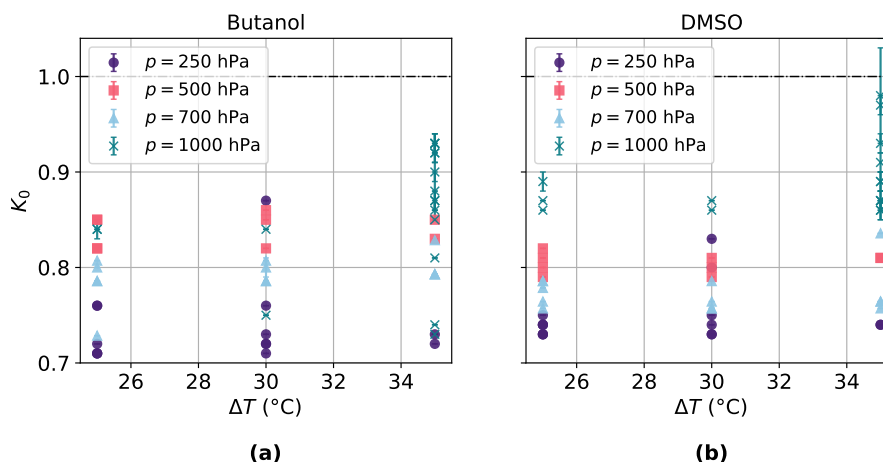


Figure 12. Calibration factor K_0 at different temperature differences between saturator and condenser for (a) the B-CPC and (b) the DMSO-CPC, serving as a relative indicator of the asymptotic maximum counting efficiency η_{\max} . K_0 shows no dependence on temperature difference but increases with pressure, indicating a decrease in η_{\max} with decreasing pressure.

380 to $D_{50}(250\text{hPa}) = 6.2\text{nm}$ and lies within the uncertainty of the experiment. Figure 12 shows the K_0 values plotted against the temperature difference and the different pressures are denoted by the different markers. Due to the imprecise sheath flow control within the electrometer, these K_0 values cannot be treated as absolute values, but rather as a relative indicator on how the asymptotic maximum counting efficiency depends on pressure. As demonstrated in Fig. 12, there is a minor dependence of K_0 on pressure for both CPCs, with reduced values as the pressure decreases. The asymptotic maximum counting efficiency, 385 η_{\max} , decreases by about 14% as $\overline{K_0}$ drops from 0.88 at 1000 hPa to 0.75 at 250 hPa.

A key finding from the pressure-dependence measurements is the close agreement between the B-CPC and the DMSO-CPC, consistent with the observations from Weber et al. (2023). Furthermore, these results align with experimental data for a CPC operated with isopropyl alcohol reported by Bezantakos and Biskos (2022). Earlier studies consistently report a critical low- 390 pressure point at which the CPC counting efficiency drops sharply (Hermann and Wiedensohler, 2001; Zhang and Liu, 1991; Hermann et al., 2005). As no such sharp drop was observed in our measurements, it is likely that the critical pressure for the Sky-CPC 5411 was not reached for either working fluid. Moreover, the pressure independence of D_{50} was confirmed for other CPC temperature settings (see Sect. 4.5).

4.4 Internal Temperature Dependence of the CPC Counting Efficiency

395 The counting efficiencies of the two Sky-CPCs 5411 (B-CPC and DMSO-CPC) were measured at five different internal temperature settings, as described in Sect. 2.1.1. The saturator and condenser temperatures are fixed values set via the CPCs' software, allowing investigation of both the temperature difference between saturator and condenser and the absolute temperatures of

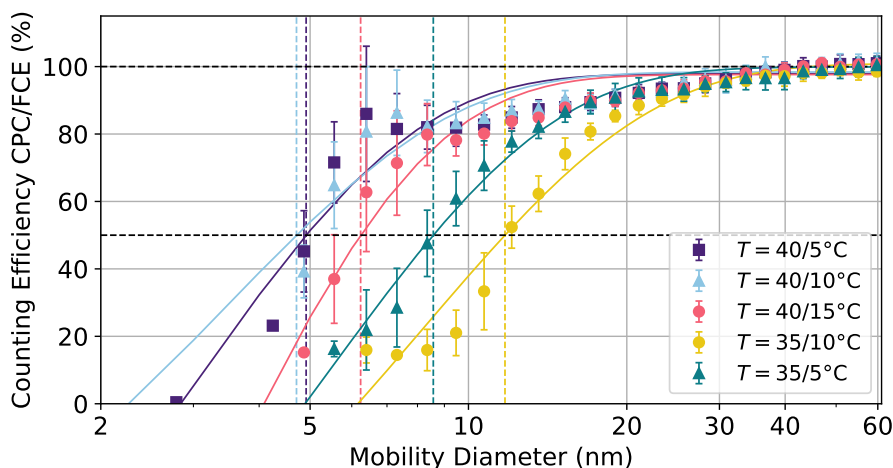


Figure 13. Counting efficiency curves of the DMSO-CPC at five internal temperature settings at 1000 hPa. Error bars represent the standard deviation of mean efficiencies. Dashed lines indicate the calculated D_{50} cutoff diameters, which shift significantly toward smaller values with increasing temperature difference and higher saturator temperatures.

each component. The chosen settings cover a temperature difference range of 25–35 °C, with saturator temperatures varying between 35 and 40 °C. Of particular interest is the setting $T_{\text{sat}} = 40\text{ °C}$ and $T_{\text{con}} = 15\text{ °C}$, since the freezing point of DMSO is 18 °C. With the condenser temperature close to the freezing point, potential differences in droplet growth — whether forming solid crystals or droplets — could be observed (Weber et al., 2023).

Figure 13 shows the counting efficiency curves of different temperature settings for the DMSO-CPC at ambient pressure of approximately 1000 hPa. As before, the y-axis error bars indicate the standard deviation of the counting efficiency mean values and the vertical dashed lines represent the calculated D_{50} cutoff diameters. It is evident that the temperature settings of the CPC have an impact on the D_{50} , with a higher temperature difference leading to lower D_{50} cutoff diameters. This finding is in good agreement with other studies and can simply be explained by higher supersaturations achieved in the condenser (Hermann and Wiedensohler, 2001; Hermann et al., 2005). Especially the reduced saturator temperature of $T_{\text{sat}} = 35\text{ °C}$ seems to lead to a more pronounced shift towards larger particle diameters than the temperature difference itself. This finding was also reported by Mei et al. (2021), who conducted a simulation study in which they varied the temperatures of the saturator and condenser of a water-based CPC, while maintaining the temperature difference constant.

The temperature setting of interest, with a condenser temperature near the freezing point of DMSO, does not show a significant difference compared to the other efficiency curves at the same saturator temperature. Consequently, it remains unclear whether droplet growth is unaffected or if the particle phase has no influence on the detection process.

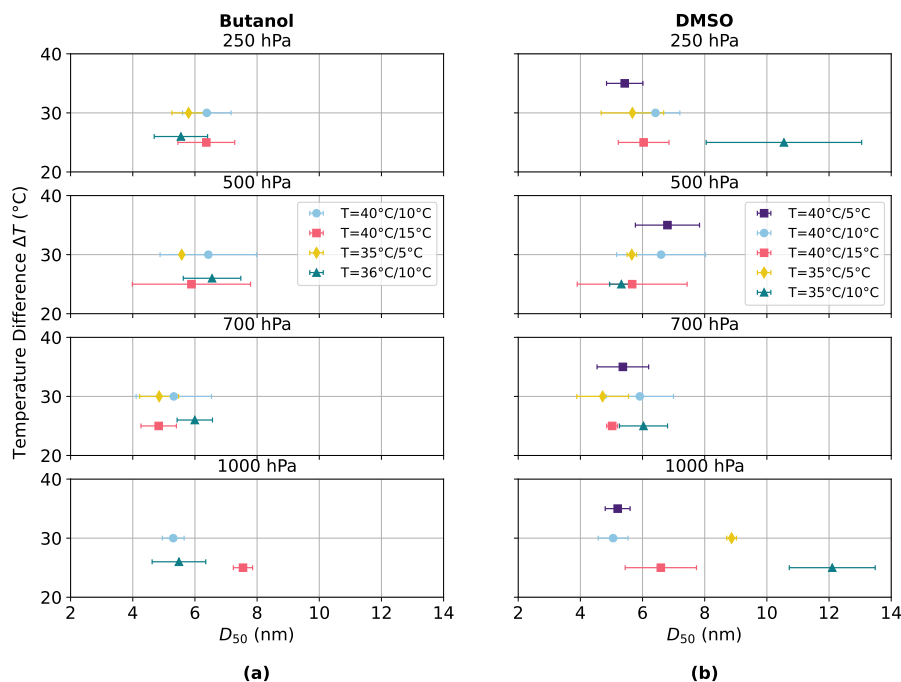


Figure 14. Comparison of D_{50} cutoff diameters at four pressures and five temperatures for (a) the B-CPC and (b) the DMSO-CPC. Data points represent the mean of multiple measurements, with error bars showing the standard deviation. For the B-CPC, $\overline{D_{50}^{\text{Butanol}}} = (5.6 \pm 0.5)$ nm. Considering only reasonable temperature settings, the DMSO-CPC yields $\overline{D_{50}^{\text{DMSO}}} = (5.8 \pm 0.9)$ nm.

In analogy to the pressure dependence, the asymptotic maximum counting efficiency η_{max} was investigated using the calibration parameter K_0 . As shown in Fig. 12, K_0 , and consequently η_{max} , exhibits no significant temperature dependence for either CPC within the range of tested temperature differences. Previous studies that examined even smaller temperature differences, however, reported a decrease in the maximum counting efficiency as the temperature difference becomes very small (Hermann and Wiedensohler, 2001; Mei et al., 2021).

4.5 Combined Dependencies and Comparison to Butanol

Figure 14 shows the combined dependencies of the averaged D_{50} cutoff diameters for both CPCs based on repeated measurements. The CPC operated with butanol exhibits only minor variations in D_{50} across all temperature settings and pressures, with an average value of $\overline{D_{50}^{\text{Butanol}}} = (5.6 \pm 0.5)$ nm. This result agrees well with the value of $D_{50} = (5.5 \pm 1.5)$ nm reported by Weber et al. (2023), measured under identical conditions for both butanol and DMSO.

In contrast, the CPC operated with DMSO shows larger variations in D_{50} with changing temperature differences and pressures. Compared to the findings of Weber et al. (2023), our measurements indicate a higher variability, with $\overline{D_{50}^{\text{DMSO}}} = (6.6 \pm 2.2)$ nm across all conditions. The temperature setting of $T_{\text{sat}} = 35^\circ\text{C}$ and $T_{\text{con}} = 10^\circ\text{C}$, in particular, results in notably larger cutoff

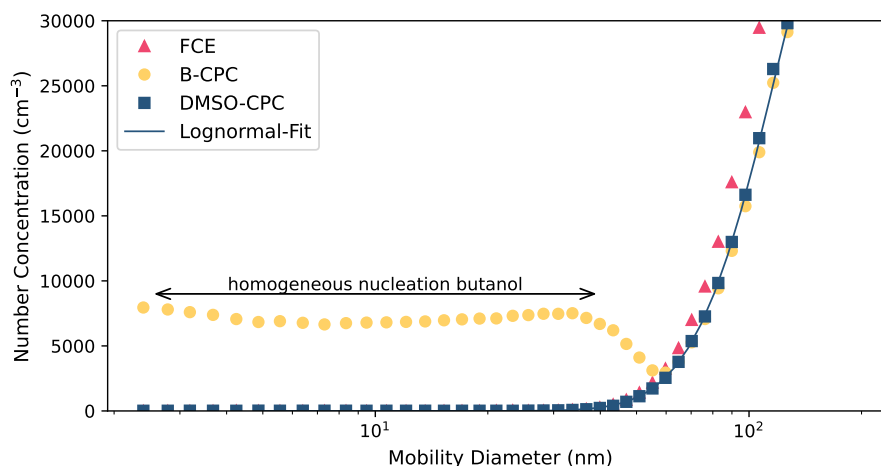


Figure 15. Uncorrected particle counts of the B-CPC, DMSO-CPC, and FCE at $T_{\text{sat}} = 40^\circ\text{C}$ and $T_{\text{con}} = 5^\circ\text{C}$. For small particle diameters, the B-CPC records non-zero counts due to homogeneous nucleation of butanol.

diameters. This can be explained by the corresponding c_1/c_0 ratios, which fall below 0.1 under these conditions, indicating insufficient particle growth. When considering only temperature settings with $c_1/c_0 > 0.2$, the mean value reduces to $\overline{D}_{50}^{\text{DMSO}} = (5.8 \pm 0.9)$ nm, which is consistent with the result obtained using the B-CPC.

435 The highest temperature difference of $\Delta T = 35^\circ\text{C}$ could not be applied to the B-CPC, as homogeneous nucleation of butanol
 was observed under this condition. Figure 15 shows the uncorrected counts of both CPCs and the FCE. In this measurement,
 both CPCs were operated at $T_{\text{sat}} = 40^\circ\text{C}$ and $T_{\text{con}} = 5^\circ\text{C}$. For smaller particle diameters, the number concentration recorded
 by the B-CPC does not decrease to zero, indicating the occurrence of homogeneous nucleation of butanol. This observation
 is consistent with the findings of Mordas et al. (2007), who reported homogeneous nucleation in a different model CPC at
 440 $\Delta T = 39^\circ\text{C}$.

At this point, it should be emphasized that the DMSO-CPC is capable of achieving results comparable to those of the B-CPC under appropriate conditions, where the c_0 adjustment is justified. Further adaptations and optimisation steps aimed at improving the performance of the DMSO-CPC are discussed in Sect. 4.9.

445 4.6 Consumption and Ambient Air Measurements during Long-Term Deployment

Long-term experiments were conducted to quantify the consumption of the working fluid. The B-CPC was operated at temperatures of $T_{\text{sat}} = 36^\circ\text{C}$ and $T_{\text{con}} = 10^\circ\text{C}$, as intended by the manufacturer. The DMSO-CPC was operated at temperatures of $T_{\text{sat}} = 40^\circ\text{C}$ and $T_{\text{con}} = 5^\circ\text{C}$, where it was found to perform best. The CPC was completely dry at the beginning of the experiment and a well known amount of working fluid was filled in the supply bottle. The CPC was considered to be dry again as soon



450 as the liquid level warning was displayed even though the CPC was still operating for several hours after the initial warning. The consumption of DMSO was calculated to be in the range of $2 - 3 \text{ mL day}^{-1}$, whereas that of butanol was determined to be 96 mL day^{-1} .

Furthermore, ambient air measurements were conducted over several days. It was observed that the DMSO-CPC did not exhibit any complications and functioned in a stable manner. Moreover, throughout the duration of the present study, the CPC operated with DMSO was utilised for a period of several months, encompassing all experiments conducted.

4.7 DMSO-H₂O Mixture

DMSO is soluble in water. The usage of a mixture of DMSO and water as working fluid brings two important advantages. First, the freezing point of DMSO of $+18^\circ\text{C}$ can be adjusted to less than -100°C by adding defined amounts of water (Havemeyer, 1966). Second, defined amounts of water also increase the flash point of DMSO from 98°C to temperatures above 140°C , as can be seen in Fig. B2 in the appendix. It depicts the pressure-dependent flash points calculated according to Astbury et al. (2004), using the experimental mole fraction data for DMSO and H₂O reported by Nishimura et al. (1972). Consequently, employing a DMSO-H₂O mixture as the working fluid enables CPC operation under extreme conditions, such as low pressures encountered during aircraft measurements or low temperatures in polar environments.

465

Figure 16 shows the results of an ambient air measurement at the campus of research center Jülich (Germany), which is located within a forest area. During this measurement the CPC was operated with a mixture of 90% DMSO and 10% water. To test the performance and duration of operation of the DMSO-H₂O-CPC, there was no automatic refilling. Panel (a) shows the c_1/c_0 ratio over time. Panel (b) depicts the number concentration measured by both CPCs, where the DMSO-H₂O data is adjusted to the c_0 threshold (see Sect. 4.1). The results show a decreasing c_1/c_0 -ratio over time, indicating that the wick inside the CPC becomes drier and the saturation for particle activation decreases. Nevertheless, the c_0 number concentration of the DMSO-H₂O-CPC is in good agreement with the B-CPC, which was operated as intended by the manufacturer. This experiment demonstrates that the DMSO-H₂O-CPC can operate accurately for at least 72 hours without requiring maintenance. Nevertheless, the option of automatic refilling further enhances its suitability, making the DMSO-H₂O-CPC ideal for deployment at remote measurement stations in challenging environments. Panel (c) depicts the correlation between the B-CPC and the DMSO-H₂O-CPC during this ambient air experiment. The slope of the linear correlation is 1.0046 ± 0.0001 ($R^2 > 0.99$, number of data points $n = 63442250$), indicating that the measurements made using DMSO-H₂O as working fluid are not distinguishable from the measurements performed with butanol.

475

4.8 Aerosol Chemical Composition Dependence

480 In order to investigate the dependence of the CPCs on the chemical composition of the aerosol, we conducted systematic measurements using three types of aerosol particles: sodium chloride (NaCl), ammonium sulfate ((NH₄)₂SO₄; AS), and soot. These seed types represent a range of hygroscopic properties and atmospheric relevance. The soot particles were generated

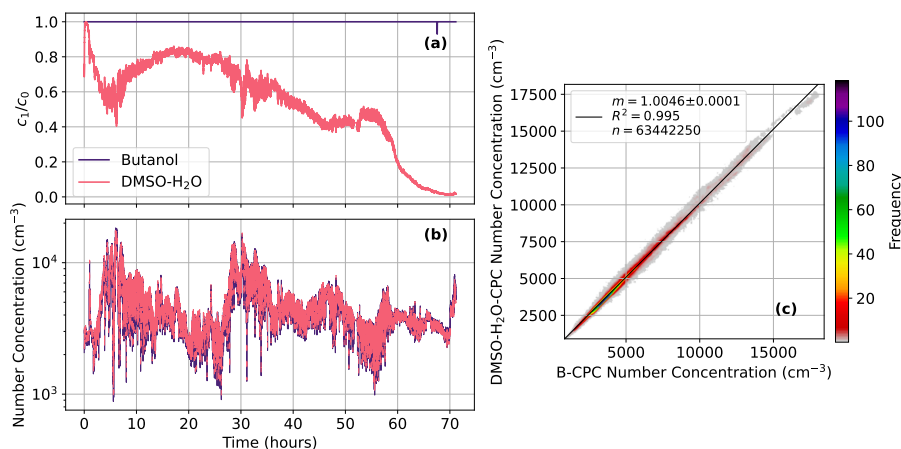


Figure 16. Ambient air measurements comparing the B-CPC and the DMSO–H₂O–CPC. Panel (a) shows the measured c_1/c_0 values for both instruments. Panel (b) presents the corresponding number concentrations over time. Panel (c) illustrates the correlation between the two CPCs, with the color scale indicating the frequency of data points within the 2σ uncertainty. The DMSO–H₂O–CPC results are statistically indistinguishable from those of the B-CPC.

using an inverted flame soot generator (see Sect. 2.1.1), producing a size distribution with a CMD around 140 nm. Due to this relatively large CMD, we are primarily sensitive to the left-hand side of the distribution, limiting the observable size range for these particles in the CPC, which could lead to a greater uncertainty of the resulting D_{50} cutoff diameters for soot particles.

Measurements were performed at two pressures, 1000 hPa and 700 hPa. For each pressure level, the CPC was operated at three different temperature settings, corresponding to a range of temperature differences between the saturator and condenser from 35 °C to 25 °C. This range allows to systematically probe the influence of supersaturation on particle activation and detection efficiency. The resulting data provide insight into how the CPC responds to particles of varying composition and size under different environmental and operational conditions. The resulting D_{50} cutoff diameters are listed in Table 3 for both CPCs.

It is evident from the data presented that there is no significant difference in the D_{50} cutoff diameter between the B-CPC and the DMSO-CPC at 700 hPa. At ambient pressures of approximately 1000 hPa the performance of the DMSO-CPC is highly depending on the temperature difference between saturator and condenser. While the cutoff diameters from the DMSO-CPC for $\Delta T = 35$ °C and $\Delta T = 30$ °C are comparable to the ones from the B-CPC, the D_{50} diameters at $\Delta T = 25$ °C are shifted towards larger diameters for the DMSO-CPC. The only exception is soot, where also at $\Delta T = 30$ °C a larger D_{50} is observed with the DMSO-CPC. Overall, however, and particularly at the highest temperature difference, the results obtained using the CPC with DMSO are comparable to those obtained using the B-CPC. This indicates that both working fluids exhibit a similar dependence on the chemical composition of the aerosol if operated under reasonable temperature settings.



Table 3. Experimentally determined D_{50} cutoff diameters (nm) for sodium chloride (NaCl), ammonium sulfate (AS), and soot particles at 1000 and 700 hPa, measured at three internal temperature settings for both the B-CPC and DMSO-CPC.

p (hPa)	T (°C)	Butanol			DMSO		
		NaCl	AS	Soot	NaCl	AS	Soot
1000	40/5	-	-	-	5.2 ± 0.4	6.8 ± 0.3	8.0 ± 0.3
	35/5	5.3 ± 0.4	7.8 ± 0.1	7.8 ± 0.2	5.1 ± 0.5	7.8 ± 0.1	11.0 ± 0.4
	35/10	6.1 ± 0.2	7.2 ± 0.5	8.4 ± 0.2	12.1 ± 1.4	13.7 ± 0.1	10.8 ± 1.2
700	40/5	-	-	-	5.4 ± 0.8	10.7 ± 0.3	13.3 ± 1.0
	40/10	5.3 ± 1.2	11.1 ± 0.2	15.5 ± 0.6	5.9 ± 1.1	11.1 ± 0.2	15.9 ± 0.7
	35/10	6.1 ± 1.1	13.2 ± 0.2	16.0 ± 0.5	6.0 ± 0.8	13.5 ± 0.2	17.2 ± 0.5

4.9 Considerations to Counterbalance Small Particle Growth

To improve the c_1/c_0 ratios under identical conditions and thus reduce the signal-to-noise ratio, the laser power for particle detection was increased. While the standard laser current of the Sky-CPC 5411 in the tested unit is approximately 24 mA, a maximum current of 28 mA was examined. At ambient pressure, this adjustment resulted in a fully stable c_1/c_0 ratio and improved linearity with respect to the reference instrument, up to concentrations of 8×10^4 particles cm^{-3} . Furthermore, reducing the flow rate from the manufacturer-specified 0.6 to 0.3 lpm enhanced linearity even further, enabling measurements exceeding 10^5 particles cm^{-3} . This indicates that the lower flow rate allows sufficient time for particle growth.

In Sect. 4.1, the lowest c_1/c_0 ratios were observed at $T_{\text{sat}} = 35^\circ\text{C}$ and $T_{\text{con}} = 10^\circ\text{C}$ at 250 hPa, as shown in Fig. 17a). This panel displays c_1/c_0 ratios as a function of total aerosol surface area. Panel b) shows results obtained under identical conditions but with increased laser power. The ratios rise dramatically — by nearly two orders of magnitude — yielding an average D_{50} cutoff diameter of (7.9 ± 0.2) nm. In comparison, the lower laser power resulted in $D_{50} = (12.1 \pm 1.4)$ nm, nearly twice as large. This finding supports the hypothesis discussed in Sect. 4.5 that low c_1/c_0 ratios lead to unrepresentative D_{50} values with increased uncertainty.

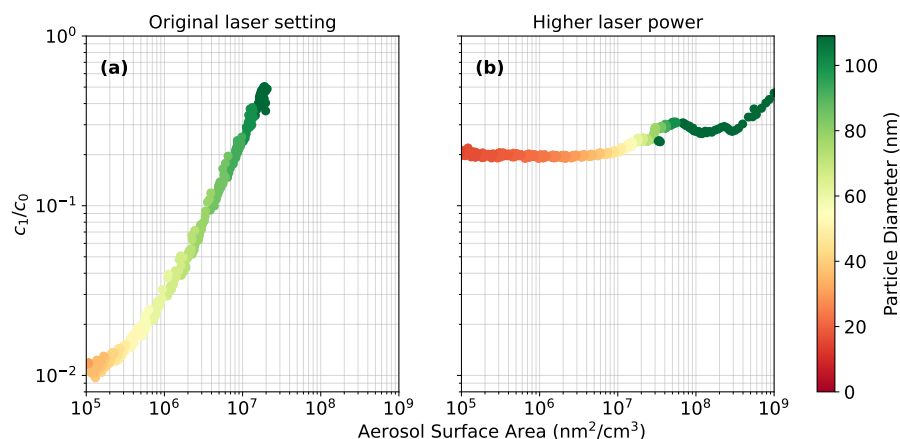


Figure 17. c_1/c_0 ratios of the DMSO-CPC at $T_{\text{sat}} = 35^\circ\text{C}$ and $T_{\text{con}} = 10^\circ\text{C}$ at 250 hPa as a function of total aerosol surface area. Panel (a): Measurement with standard laser power. Panel (b): Same conditions with increased laser power, showing a nearly two-order-of-magnitude rise in c_1/c_0 .

5 Conclusions

This study presents a comprehensive laboratory and field-based evaluation of dimethyl sulfoxide (DMSO) as a non-flammable working fluid for the Sky-CPC 5411 (GRIMM Aerosol Technik), directly compared with a butanol-operated counterpart across a wide range of operational pressures, temperature settings, and aerosol types. To enable the use of the instrument's automatic
520 refilling process, the automatic refilling valve was modified. These modifications were straightforward to implement and ensured reliable refilling over a period of six months of intermittent operation.

This study demonstrates that droplet growth in the DMSO-CPC strongly depends on the saturator temperature T_{sat} and the temperature difference between saturator and condenser ΔT . Optimal growth, indicated by c_1/c_0 ratios near unity, occurs at
525 high T_{sat} and large ΔT , while lower temperatures or smaller differences reduce growth, particularly at 1000 hPa and 250 hPa. Portable Optical Particle Counter (POPS) measurements confirmed that increasing ΔT enhances droplet sizes. Simulations of the saturation inside the condenser reproduced the pressure- and temperature-dependent trends, showing that both the position and magnitude of the maximum saturation ratio S_{max} determine the activation of the smallest particles. Overall, the results highlight the importance of CPC internal settings for reliable particle activation and provide guidance for optimising DMSO-
530 CPC operation under varying environmental conditions.

The DMSO-CPC achieved counting efficiencies and cutoff diameters comparable to those of the Butanol-CPC, with an overall average of $\overline{D_{50}^{\text{DMSO}}} = (5.8 \pm 0.9)$ nm compared to $\overline{D_{50}^{\text{Butanol}}} = (5.6 \pm 0.5)$ nm. While the Butanol-CPC demonstrated stable performance across all pressures and temperature settings, the DMSO-CPC exhibited a stronger sensitivity to internal temperatures,



535 with smaller temperature differences leading to larger D_{50} cutoffs. The asymptotic maximum counting efficiency showed only
a minor pressure dependence, decreasing by about 14% between 1000 and 250 hPa.

Furthermore, the use of DMSO substantially reduced working fluid consumption (2–3 mL day⁻¹ compared to 96 mL day⁻¹
for butanol), and long-term ambient air measurements confirmed stable and reliable operation over several months. Exper-
540 iments with a DMSO–H₂O mixture further extended the operational range of the CPC by lowering the freezing point and
improving safety margins, making the DMSO–H₂O-CPC particularly suitable for airborne applications and remote monitoring
stations under challenging environmental conditions.

Although limited droplet growth under certain settings introduced uncertainty in cutoff diameter determination, adjustments
545 such as increased laser power and reduced flow rate effectively shifted the D_{50} to lower values.

Overall, the results demonstrate close agreement between the butanol- and DMSO-based CPC measurements. We conclude,
employing DMSO or DMSO–H₂O mixtures as working fluids enables safe, efficient, and regulation-compliant CPC operation
without compromising measurement quality, even under low-pressure or low-temperature conditions and in remote environ-
550 ments.



Appendix A: Recommendations

Based on the findings presented in this study, the following recommendations are provided to support the successful and safe implementation of Dimethyl Sulfoxide (DMSO) as a working fluid in Condensation Particle Counters (CPCs), particularly the GRIMM Sky-CPC 5411 model.

555 Instrument Preparation and Modifications

- **Automatic Refilling System:** The refilling valve must be adapted to ensure reliable operation with DMSO. The modification includes a replacement of the rubber O-ring with a silicon O-ring and the trimming of the rubber part of the stamp. Those steps are straightforward and essential for long-term stability.
- **Material Compatibility:** Prior to operation, all tubing, seals, and fluid-contact components should be verified for chemical compatibility with DMSO. Rubber materials should be avoided.

Operational Conditions

- **Temperature Settings:** The performance of the DMSO-CPC is more sensitive to the condenser–saturator temperature difference (ΔT) than a Butanol-CPC. A high ΔT of 35 °C ($T_{\text{sat}} = 40$ °C and $T_{\text{con}} = 5$ °C) is recommended to ensure sufficient particle activation and stable counting efficiency.
- **Flow Rate Optimization:** Reduced sample flow rates, down to 0.3L/min, can be applied to compensate for insufficient activation.
- **Laser Power Tuning:** An increased laser power, up to 28 mA, can be applied to reduce the D_{50} cutoff diameter without compromising the lifetime of the laser itself.

Working Fluid Handling

- **Pure DMSO Operation:** For standard laboratory use, pure DMSO offers stable performance with low fluid consumption and minimal maintenance requirements.
- **DMSO–H₂O Mixtures:** For field or airborne applications, mixtures with up to 10% water are recommended to lower the freezing point and enhance the flash point.

Hardware Adjustments

575 Based on our findings, we propose two possible modifications at the CPCs hardware in order to further optimise the performance of the CPC operated with DMSO .

- **Threshold Adjustment:** The voltage thresholds $Th(c_1)$ and $Th(c_0)$ embedded in the instruments hardware would need to be adapted for DMSO to account for its lower vapour pressure.



- 580
- **Automated Refilling:** The automatic wetting of the wick within the saturator should be optimised. It is hypothesised that a change of the liquid sensor or an adjustment in its settings would enhance the particle growth.



Appendix B: Figures

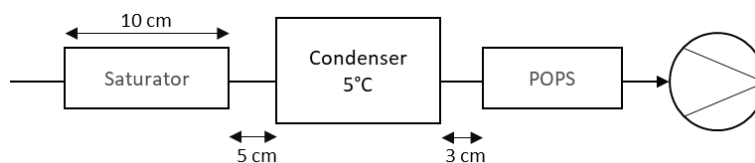


Figure B1. Flow schematic of the laboratory setup for the quantification of the final particle size in the CPC.

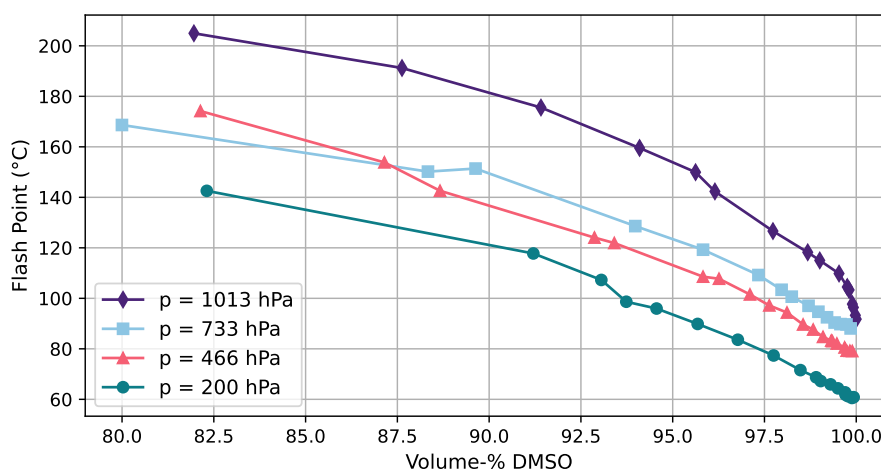


Figure B2. The dependence of the flash point on the volumetric fraction of DMSO in DMSO-H₂O mixtures for varying pressure levels (color code).



Code availability. The analysis scripts used in this study relied exclusively on standard Python libraries.

Data availability. Upon request.

Author contributions. PW and SK conceived of the study. SK performed all experiments and data analysis. PW, UB and OFB set up the
585 instruments. UB and PW designed the LabVIEW™ environment of the experimental set-up. VMF, HK and AB performed the numerical
simulations. GS, CK and LK contributed to the tuning of the CPC. SK wrote the manuscript with assistance of all other authors.

Competing interests. GS, CK, and LK are employed full-time by GRIMM Aerosol Technik GmbH, which may hold direct or indirect
financial interests related to the work presented in this paper.

Acknowledgements. Financial support by both the HITEC Graduate School (SK) and the Innovation Fund at Forschungszentrum Jülich (PW)
590 is gratefully acknowledged.



References

- Aalto, P., Hämeri, K., Paatero, P., Kulmala, M., Bellander, T., Berglind, N., Bouso, L., Castaño-Vinyals, G., Sunyer, J., Cattani, G., Marconi, A., Cyrus, J., von Klot, S., Peters, A., Zetzsche, K., Lanki, T., Pekkanen, J., Nyberg, F., Sjövall, B., and Forastiere, F.: Aerosol Particle Number Concentration Measurements in Five European Cities Using TSI-3022 Condensation Particle Counter over a Three-Year Period during Health Effects of Air Pollution on Susceptible Subpopulations, *Journal of the Air & Waste Management Association*, 55, 1064–1076, <https://doi.org/10.1080/10473289.2005.10464702>, 2005.
- Alam, A., Shi, J. P., and Harrison, R. M.: Observations of new particle formation in urban air, *Journal of Geophysical Research: Atmospheres*, 108, <https://doi.org/https://doi.org/10.1029/2001JD001417>, 2003.
- Astbury, G. R., Bugand-Bugandet, J., Grollet, E., and Stell, K. M.: Flash points of aqueous solutions of flammable solvents, 2004.
- Balendra, S., Kale, A., Pongetti, J., Kazemianesh, M., Haugen, M., Weller, L., and Boies, A.: Condensation particle counters: Exploring the limits of miniaturisation, *Journal of Aerosol Science*, 175, 106 266, <https://doi.org/10.1016/j.jaerosci.2023.106266>, 2024.
- Bauer, P. S., Spät, D., Eisenhut, M., Gattringer, A., and Weinzierl, B.: Pressure-dependent performance of two CEN-specified condensation particle counters, *Atmospheric Measurement Techniques*, 16, 4445–4460, <https://doi.org/10.5194/amt-16-4445-2023>, 2023.
- Bezantakos, S. and Biskos, G.: Temperature and pressure effects on the performance of the portable TSI 3007 condensation particle counter: Implications on ground and aerial observations, *Journal of Aerosol Science*, 159, 105 877, <https://doi.org/10.1016/j.jaerosci.2021.105877>, 2022.
- Bischof, O. F.: Application-specific calibration of condensation particle counters under low pressure conditions: = Anwendungsspezifische Kalibrierung von Kondensationspartikelzählern unter Niederdruckbedingungen, no. Band/volume 579 in *Schriften des Forschungszentrums Jülich Reihe Energie & Umwelt, energy & environment*, Forschungszentrum Jülich GmbH, Zentralbibliothek, Verlag, Aachen, ISBN 978-3-95806-629-8, 2022.
- Bundke, U., Berg, M., Houben, N., Ibrahim, A., Fiebig, M., Tettich, F., Klaus, C., Franke, H., and Petzold, A.: The IAGOS-CORE aerosol package: instrument design, operation and performance for continuous measurement aboard in-service aircraft, *Tellus B: Chemical and Physical Meteorology*, 67, 28 339, <https://doi.org/10.3402/tellusb.v67.28339>, 2015.
- Cozic, J., Verheggen, B., Mertes, S., Connolly, P., Bower, K., Petzold, A., Baltensperger, U., and Weingartner, E.: Scavenging of black carbon in mixed phase clouds at the high alpine site Jungfrauoch, *Atmospheric Chemistry and Physics Discussions*, pp. 11 877–11 912, 2006.
- Gao, R. S., Telg, H., McLaughlin, R. J., Ciciora, S. J., Watts, L. A., Richardson, M. S., Schwarz, J. P., Perring, A. E., Thornberry, T. D., Rollins, A. W., Markovic, M. Z., Bates, T. S., Johnson, J. E., and Fahey, D. W.: A light-weight, high-sensitivity particle spectrometer for PM_{2.5} aerosol measurements, *Aerosol Science and Technology*, 50, 88–99, 2016.
- Hao, W., Stolzenburg, M., Attoui, M., Zhang, J., and Wang, Y.: Optimizing the activation efficiency of sub-3 nm particles in a laminar flow condensation particle counter: Model simulation, *Journal of Aerosol Science*, 158, 105 841, <https://doi.org/10.1016/j.jaerosci.2021.105841>, 2021.
- Havemeyer, R. N.: Freezing Point Curve of Dimethyl Sulfoxide—Water Solutions, *Journal of Pharmaceutical Sciences*, 55, 851–853, <https://doi.org/10.1002/jps.2600550822>, publisher: Elsevier BV, 1966.
- Hermann, M. and Wiedensohler, A.: Counting efficiency of condensation particle counters at low-pressures with illustrative data from the upper troposphere, *Journal of Aerosol Science*, 32, 975–991, 2001.
- Hermann, M., Adler, S., Caldow, R., Stratmann, F., and Wiedensohler, A.: Pressure-dependent efficiency of a condensation particle counter operated with FC-43 as working fluid, *Journal of Aerosol Science*, 36, 1322–1337, <https://doi.org/10.1016/j.jaerosci.2005.03.002>, 2005.



- IPCC: Climate Change 2021: The Physical Science Basis. Contribution of Working Group I to the Sixth Assessment Report of the Intergovernmental Panel on Climate Change, vol. In Press, Cambridge University Press, Cambridge, United Kingdom and New York, NY, USA, <https://doi.org/10.1017/9781009157896>, 2021.
- Jarrett, D. G. and Owen, M. C.: Traceability for Aerosol Electrometer in the fA Range, 2013.
- Jurányi, Z., Gysel, M., Weingartner, E., DeCarlo, P. F., Kammermann, L., and Baltensperger, U.: Measured and modelled cloud condensation nuclei number concentration at the high alpine site Jungfraujoch, *Atmospheric Chemistry and Physics*, 10, 7891–7906, <https://doi.org/10.5194/acp-10-7891-2010>, 2010.
- Kahn, R. A., Andrews, E., Brock, C. A., Chin, M., Feingold, G., Gettelman, A., Levy, R. C., Murphy, D. M., Nenes, A., Pierce, J. R., Popp, T., Redemann, J., Sayer, A. M., Da Silva, A. M., Sogacheva, L., and Stier, P.: Reducing Aerosol Forcing Uncertainty by Combining Models With Satellite and Within-The-Atmosphere Observations: A Three-Way Street, *Reviews of Geophysics*, 61, e2022RG000796, <https://doi.org/10.1029/2022RG000796>, 2023.
- Kim, W. Y., Lee, S. G., Lee, H., and Ahn, K.-H.: Investigation of Vertical Profiles of Particulate Matter and Meteorological Variables up to 2.5 km in Altitude Using a Drone-Based Monitoring System, *Atmosphere*, 16, 2025.
- Krasa, H., Fruhmann, V. M., Schurl, S., Kupper, M., and Bergmann, A.: Condensation diffusion charging – particle number measurement of high concentrations down to 3 nm, *Aerosol Research*, 3, 521–534, <https://doi.org/10.5194/ar-3-521-2025>, 2025.
- Kulkarni, P., Baron, P. A., and Willeke, K.: *Aerosol Measurement: Principles, Techniques, and Applications*, 3rd edition, John Wiley & Sons Ltd, 2011.
- Laj, P., Lund Myhre, C., Riffault, V., Amiridis, V., Fuchs, H., Eleftheriadis, K., Petäjä, T., Salameh, T., Kivekäs, N., Juurola, E., Saponaro, G., Philippin, S., Cornacchia, C., Alados Arboledas, L., Baars, H., Claude, A., De Mazière, M., Dils, B., Dufresne, M., Evangeliou, N., Favez, O., Fiebig, M., Haeffelin, M., Herrmann, H., Höhler, K., Illmann, N., Kreuter, A., Ludewig, E., Marinou, E., Möhler, O., Mona, L., Eder Murberg, L., Nicolae, D., Novelli, A., O’Connor, E., Ohneiser, K., Petracca Altieri, R. M., Picquet-Varrault, B., Van Pinxteren, D., Pospichal, B., Putaud, J.-P., Reimann, S., Siomos, N., Stachlewska, I., Tillmann, R., Voudouri, K. A., Wandinger, U., Wiedensohler, A., Apituley, A., Comerón, A., Gysel-Ber, M., Mihalopoulos, N., Nikolova, N., Pietruczuk, A., Sauvage, S., Sciare, J., Skov, H., Svendby, T., Swietlicki, E., Tonev, D., Vaughan, G., Zdimal, V., Baltensperger, U., Doussin, J.-F., Kulmala, M., Pappalardo, G., Sorvari Sundet, S., and Vana, M.: Aerosol, Clouds and Trace Gases Research Infrastructure (ACTRIS): The European Research Infrastructure Supporting Atmospheric Science, *Bulletin of the American Meteorological Society*, 105, E1098–E1136, <https://doi.org/10.1175/BAMS-D-23-0064.1>, 2024.
- Lee, L. A., Reddington, C. L., and Carslaw, K. S.: On the relationship between aerosol model uncertainty and radiative forcing uncertainty, *Proceedings of the National Academy of Sciences*, 113, 5820–5827, <https://doi.org/10.1073/pnas.1507050113>, 2016.
- Lewis, G. S. and Hering, S. V.: Minimizing Concentration Effects in Water-Based, Laminar-Flow Condensation Particle Counters, *Aerosol Science and Technology*, 47, 645–654, <https://doi.org/10.1080/02786826.2013.779629>, 2013.
- Maring, H. and Schwartz, G.: A condensation particle counter for long-term continuous use in the remote marine environment, *Atmospheric Environment*, 28, 3293–3298, 1994.
- McNeill, V. F.: Atmospheric Aerosols: Clouds, Chemistry, and Climate, *Annual Review of Chemical and Biomolecular Engineering*, 8, 427–444, <https://doi.org/10.1146/annurev-chembioeng-060816-101538>, 2017.
- Mei, F., Spielman, S., Hering, S., Wang, J., Pekour, M. S., Lewis, G., Schmid, B., Tomlinson, J., and Havlicek, M.: Simulation-aided characterization of a versatile water-based condensation particle counter for atmospheric airborne research, *Atmospheric Measurement Techniques*, 14, 7329–7340, <https://doi.org/10.5194/amt-14-7329-2021>, 2021.



- Mordas, G., Sipilä, M., and Kulmala, M.: Nanoparticle Detection Using Nucleation Regime of the CPC, in: *Nucleation and Atmospheric Aerosols*, edited by O'Dowd, C. D. and Wagner, P. E., pp. 209–213, Springer Netherlands, Dordrecht, ISBN 978-1-4020-6474-6 978-1-4020-6475-3, https://doi.org/10.1007/978-1-4020-6475-3_43, 2007.
- Nishimura, M., Nakayama, M., and Yano, T.: VAPOR PRESSURE OF PURE DMSO AND VAPOR-LIQUID EQUILIBRIA IN
670 DMSO-H₂O SYSTEM UNDER ISOBARIC CONDITIONS, *JOURNAL OF CHEMICAL ENGINEERING OF JAPAN*, 5, 223–226,
<https://doi.org/10.1252/jcej.5.223>, 1972.
- OJ EU, 2024/2881: ELI: <http://data.europa.eu/eli/dir/2024/2881/oj>.
- Pandis, J. H. and Pandis, S. N.: *Atmospheric Chemistry and Physics: From Air Pollution to Climate Change*, 3rd edn., Wiley-VCH, New York, ISBN 978-1-118-94740-1, 2016.
- 675 Petzold, A., Thouret, V., Gerbig, C., Zahn, A., Brenninkmeijer, C. A. M., Gallagher, M., Hermann, M., Pontaud, M., Ziereis, H., Boulanger, D., Marshall, J., Nédélec, P., Smit, H. G. J., Friess, U., Flaud, J.-M., Wahner, A., Cammas, J.-P., Volz-Thomas, A., and Team, I.: Global-scale atmosphere monitoring by in-service aircraft – current achievements and future prospects of the European Research Infrastructure IAGOS, *Tellus B: Chemical and Physical Meteorology*, 67, 28 452, <https://doi.org/10.3402/tellusb.v67.28452>, 2015.
- Polyanskiy, M. N.: Refractiveindex.info database of optical constants, *Scientific Data*, 11, <https://doi.org/10.1038/s41597-023-02898-2>,
680 2024.
- Pöschl, U.: *Atmospheric Aerosols: Composition, Transformation, Climate and Health Effects*, *Angewandte Chemie International Edition*, 44, 7520–7540, <https://doi.org/10.1002/anie.200501122>, publisher: Wiley, 2005.
- Watson-Parris, D. and Smith, C. J.: Large uncertainty in future warming due to aerosol forcing, *Nature Climate Change*, 12, 1111–1113, <https://doi.org/10.1038/s41558-022-01516-0>, 2022.
- 685 Weber, P., Bischof, O. F., Fischer, B., Berg, M., Hering, S., Spielman, S., Lewis, G., Petzold, A., and Bundke, U.: Characterisation of a self-sustained, water-based condensation particle counter for aircraft cruising pressure level operation, *Atmospheric Measurement Techniques*, 16, 3505–3514, <https://doi.org/10.5194/amt-16-3505-2023>, 2023.
- Wendisch, M. and Brenguier, J.-L.: *Airborne Measurements for Environmental Research*, John Wiley & Sons Ltd, 2013.
- Wiedensohler, A., Wiesner, A., Weinhold, K., Birmili, W., Hermann, M., Merkel, M., Müller, T., Pfeifer, S., Schmidt, A., Tuch, T., Velarde, F., Quincey, P., Seeger, S., and Nowak, A.: Mobility particle size spectrometers: Calibration procedures and measurement uncertainties,
690 *Aerosol Science and Technology*, 52, 146–164, <https://doi.org/10.1080/02786826.2017.1387229>, 2018.
- Yaws, C. L.: *Yaws' handbook of thermodynamic and physical properties of chemical compounds: physical, thermodynamic and transport properties for 5,000 organic chemical compounds*, 1st edn., Knovel, ISBN 978-1-59124-444-8, 2003.
- Zhang, Z. and Liu, B. Y. H.: Performance of TSI 3760 Condensation Nuclei Counter at Reduced Pressures and Flow Rates, *Aerosol Science and Technology*, 15, 228–238, <https://doi.org/10.1080/02786829108959530>, 1991.
695
- Zhang, Z. Q. and Liu, B. Y. H.: Dependence of the Performance of TSI 3020 Condensation Nucleus Counter on Pressure, Flow Rate, and Temperature, *Aerosol Science and Technology*, 13, 493–504, <https://doi.org/10.1080/02786829008959464>, 1990.